Proceedings of the IEEE Transactions on Power Electronics (TPEL)

On the Size and Weight of Passive Components: Scaling Trends for High-Density Power Converter Designs

Nathan C. Brooks
Jiarui Zou
Samantha Coday
Ting Ge
Nathan M. Ellis
R. C. N. Pilawa-Podgurski

On the Size and Weight of Passive Components: Scaling Trends for High-Density Power Converter Designs

Nathan C. Brooks, *Member, IEEE,* Jiarui Zou, *Student Member, IEEE,* Samantha Coday, *Member, IEEE,* Ting Ge, *Member, IEEE,* Nathan M. Ellis, *Member, IEEE,* and Robert C. N. Pilawa-Podgurski, *Fellow, IEEE*

***Abstract*—High performance power electronics design requires a firm characterization of active and passive components. This work presents a framework for quantifying passive component performance by reviewing both existing methods and robust device figures-of-merit. A comprehensive survey yields aggregated data for nearly 700,000 commercial capacitors and inductors of all types. To supplement deficiencies in this data, this work proposes and validates several empirical expressions to estimate passive component energy storage and mass. Estimation of volumetric mass density per component type allows the approximation of component mass from accessible box volume. Estimation of energy-equivalent capacitance in nonlinear Class II ceramic capacitors facilitates the evaluation of stored energy and related energy density figures-of-merit. A phenomenological analysis of the comprehensive component data produces several conclusory determinations about peak energy density capabilities—with respect to volume, mass, and cost—across capacitor and inductor technologies.**

***Index Terms*—capacitor, Class II ceramic capacitor, inductor, device figure-of-merit, device characterization, component volumetric density, component energy density, data collection, passive component survey, overrating**

I. Introduction

MODERN power electronic converters comprise active semiconductor devices (e.g., diodes and transistors), and passive devices to electromagnetically store and release energy (e.g., capacitors, inductors, transformers). A comprehensive understanding of the breadth and capabilities of these devices is required to design and realize a physical converter of desired conversion efficiency, volume, mass, cost, lifetime, and dynamic performance. Both novel and mature component technologies constantly improve over time, and the best-suited device for a particular application depends on the system specification and, even more intricately, on other selected devices.

The choice of optimal circuit topology varies when scrutinizing the passive devices in particular. The most mature switched-mode circuit topologies primarily rely on inductors for energy storage (e.g., buck; boost; buck-boost; flyback; and dual-active bridge, DAB, converters). Since they are difficult to miniaturize [1], inductors continue to demand intense research focus for the device-level design of power converters. The comparably lower losses and higher energy densities of capacitors [2]–[4] have motivated the investigation and development of more inductive/capacitive circuit topologies in recent decades: multilevel converters [5] (e.g., modular multilevel converter, MMC [6]–[8]; flying capacitor multilevel, FCML, converter [9]–[11]); hybrid switched capacitor converters [12]–[15] (e.g., series-capacitor buck [16]–[18]); and isolated resonant converters [19] (e.g. series-resonant [20], [21]; LLC [22], [23]). These families of power converter topologies are each high-performance and can maximally utilize the energy storage and power throughput capabilities of both capacitors and inductors.

This work extends our previous conference paper [4] by aggregating a comprehensive set of capacitor and inductor device data and motivating useful figures-of-merit (FOM) for comparison and extension to design. The primary research contributions of this work are as follows: Section II describes general methods for device-level characterization and introduces a framework for producing robust, or maximally applicable, device FOM. Employing comprehensive data collection, this work surveys a useful breadth of over 606,000 commercial capacitors and 88,000 commercial inductors as detailed in Section III. Additional sampled data is garnered to supplement and augment particular deficiencies in this large data set. To enable complete characterization of energy storage metrics—the critical benchmark of capacitive and inductive energy storage elements—a sampled set of capacitor data is collected and extrapolated to the full data set as described in Section IV. To estimate component mass, a sampled set of components is measured and extrapolated to the full data set as described in Section V. After applying the supplements to energy storage and mass, Section VI explores the veracity of the data through visualization and investigates several device FOM for all surveyed components. As a demonstration, the analysis compares the energy densities of various capacitor and

Manuscript received XXXXXXX; accepted XXXXXXXX. This manuscript in Section V reports additional measurements for capacitor and inductor volumetric mass presented at the 2022 IEEE 23rd Workshop on Control and Modeling for Power Electronics (COMPEL) [DOI: 10.1109/COMPEL53829.2022.9829957]. This manuscript also introduces an empirically supported dc energy analysis of Class II ceramic capacitors, presents a framework for constructing useful device figures-of-merit (FOM), and applies these FOM to a large-scale component survey. *(Corresponding author: Robert Carl Nikolai Pilawa-Podgurski.)*

The authors are affiliated with the Department of Electrical Engineering and Computer Sciences, University of California, Berkeley, the Department of Electrical and Computer Engineering, Rose-Hulman Institute of Technology, and the Department of Electrical Engineering and Computer Science, Massachusetts Institute of Technology (e-mail: brooksnc@rose-hulman.edu; jiarui.zou@berkeley.edu; coday@mit.edu; gting@vt.edu; nathanmilesellis@berkeley.edu; pilawa@berkeley.edu).

Color versions of one or more of the figures in this paper are available online at http://ieeexplore.ieee.org.

inductor technologies and additionally specifies the conditions for voltage overrating in capacitors and current overrating in inductors.

II. Characterizing Components and Defining Performance

Making reductive determinations from millions of passive components requires careful consideration of how data is collected and then manipulated into useful quantitative metrics that describe comparative performance trade-offs. The goal is to produce founded statements such as "based on the present available technology, the smallest possible capacitor solution for this application has volume X." To substantiate these claims, this work first introduces viable methods of data aggregation and analysis, then motivates useful device FOM.

A. Data Analysis Methods

There are three general methods to determine the broad capabilities of a set of circuit components, where sets are classified by the distinctive 'type' or 'technology' of the component.

1) Analytically derived performance: Utilizing a first principles approach based in physics, one can derive analytical expressions for the lumped circuit model from its internal geometries and constituent material properties. Further determinations are either made directly from the analytical expressions, iteratively fit to measured data, or generated using a probabilistic Monte Carlo simulation. Examples of analytic methods include estimation of the 'macroscopic' hysteretic losses of Class II ceramic capacitors from 'microscopic' properties in [24]–[26]; quality factor prediction of air core inductors in [27]; derivation of frequency-dependent volume and loss scaling trends in inductors in [1]; and estimation of parasitics for transistors in [28].

2) Sampled data and extrapolation: Data collection, often measured, can completely characterize circuit phenomenon for small data sets. However for large sets of intractable or unknown data, intelligent data sampling can yield exceedingly meaningful qualitative and quantitative insight. With additional care, the sampled data extrapolates to larger supersets of data—especially with the advent of recent machine-learning (ML) techniques. This sampled data method is applied to predict capacitor ESR and quality factor in [3], [29]; capacitor lifetime in [30]–[32]; power loss in inductors in [27], [33]; and power FET losses in [28], [34]. Another variation of this sampled data approach trains ML models to predict core losses in broadly excited inductors [35], [36] and to predict losses in transistors [37].

3) Comprehensive data collection: Electronics distributors and even some manufacturers/suppliers have in recent years drastically broadened the interactivity of their consumer-facing interfaces and design tools. This proliferation of digitized data and its increasing ease of access enables large-scale, comprehensive, and practically exhaustive collection of component information. A comprehensive consideration of data necessarily enables conclusive interpolative—rather than extrapolative—quantification of performance, even notoriously mercurial metrics such as cost. A comprehensive data collection approach in [38] is used to benchmark performance amongst commercial high power transistor technologies ($> 1\,\mathrm{kV}$ and $> 1\,\mathrm{kA}$). A recent approach in [37] uses data from commercial capacitors, inductors, and transistors to train ML models and produce optimal converter designs [39].

This work primarily employs the *comprehensive data collection* approach for device characterization. In aspects where this method stalls, *sampled data and extrapolation* is utilized to augment the comprehensive data set.

B. Defining Useful Device Figures-of-Merit

Meaningful device metrics, deemed figures-of-merit (FOM), must be developed in conjunction with bulk device characterization. A good FOM is a quantitative measure of performance and indisputably indicates better performance for larger (or smaller) values, similar performance for equivalent values, and worse performance for smaller (or larger) values. Although not often accentuated, the FOM philosophy intrinsically permeates the field of engineering and enables quantitative benchmark and comparison of complex systems [40]. These metrics provide a common language for engineers to judge a solution's capabilities or the evolution of a technology [41]. Applied to power electronics—a system comprised of many smaller subsystems—it is possible in principal to relate converter-level FOM to constituent device-level FOM to constituent material-level FOM [28], [42].

The 'system scope' in this work is a discrete passive component. Others have motivated specific FOM for quantifying the performance of individual electronic devices: capacitors [43], inductors [33], and transistors [28], [44], with the intention of characterizing component application to larger circuits, however, no work has generalized a method for conceiving useful device FOM.

To accomplish this, consider how these devices are utilized. Two-terminal passive devices are commonly configured into series and/or parallel connected component banks to meet specified requirements often relating to energy storage or power throughput. Series-parallel modularity is even common for electrical systems such as power conversion circuits [40], [45] and photovoltaic (PV) panels [46], [47]. Consequently, any metric defined as a FOM in this work critically adheres to the following proposed property:

> **Property of Series-Parallel Modular Invariance:** A device metric invariant to series and/or parallel configuration of the device.

If a metric adheres to this property, then it is a FOM that can fairly compare devices of various voltage and current ratings and is deemed 'robust'.

The series-parallel modular invariance property is demonstrated schematically in Fig. 1 and generalized in Table I for a series and parallel configuration of a capacitor with specified capacitance C, rated dc voltage V_r, rated rms current I_r, equivalent series resistance ESR, box volume, cost, and mass. In this context, combinations of these base attributes yield some robust FOM which satisfy this property and are agnostic to both series and parallel component configurations—e.g.,

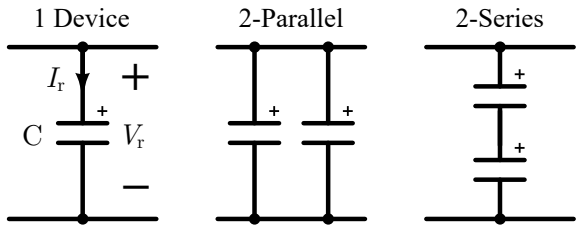

Fig. 1. Schematic denoting series and parallel bank configurations of a capacitor component.

TABLE I
GENERIC CAPACITOR BANK SPECIFICATIONS AND CONSTRUCTED FIGURES-OF-MERIT

Total Specification	1 Device	2-Parallel	2-Series	n-Series/ m-Parallel
C_tot	C	$2C$	$\frac{1}{2}C$	$\frac{m}{n}C$
$V_\mathrm{r,tot}$	V_r	V_r	$2V_\mathrm{r}$	nV_r
$I_\mathrm{r,tot}$	I_r	$2I_\mathrm{r}$	I_r	mI_r
$\mathrm{ESR}_\mathrm{tot}$	ESR	$\frac{1}{2}$ESR	2 ESR	$\frac{n}{m}$ESR
$\mathrm{Vol}_\mathrm{tot}$	Vol	2 Vol	2 Vol	nm Vol
$\mathrm{Mass}_\mathrm{tot}$	Mass	2 Mass	2 Mass	nm Mass
$\mathrm{Cost}_\mathrm{tot}$	Cost	2 Cost	2 Cost	nm Cost
$E_\mathrm{r,tot} = \frac{1}{2}CV_\mathrm{r}^2$	E_r	$2E_\mathrm{r}$	$2E_\mathrm{r}$	nmE_r
$P_\mathrm{r,tot} = V_\mathrm{r}I_\mathrm{r}$	P_r	$2P_\mathrm{r}$	$2P_\mathrm{r}$	nmP_r
$\gamma_\mathrm{v,tot} = \frac{E_\mathrm{r,tot}}{\mathrm{Vol}_\mathrm{tot}}$	γ_v	γ_v	γ_v	γ_v
$\rho_\mathrm{m,tot} = \frac{P_\mathrm{r,tot}}{\mathrm{Mass}_\mathrm{tot}}$	ρ_m	ρ_m	ρ_m	ρ_m
$(\tan\delta)_\mathrm{tot} = \omega C\,\mathrm{ESR}$	$\tan\delta$	$\tan\delta$	$\tan\delta$	$\tan\delta$

volumetric energy density γ_v, gravimetric power density ρ_m, and loss tangent $\tan\delta$ (or dissipation factor DF).

C. Examples of Robust FOM

Conventional *capacitor* FOM satisfying the series-parallel modular invariance property include charge-discharge efficiency $\frac{E_\mathrm{discharge}}{E_\mathrm{charge}}$ [48]–[50]; loss tangent or dissipation factor $\tan\delta$ or quality factor $Q = \frac{1}{\tan\delta}$ [29], [48], [51]; dielectric loss density $\frac{P_\mathrm{loss}}{\mathrm{Vol}}$ [25]; the Ohms-Farad product $C \cdot \mathrm{ESR}$ [43], [48]; packaging efficiency, the proportion of active volume within the device to total device volume [43], [52]; energy density of the dielectric material [49], [53]–[55]; energy density of the whole capacitor $\frac{E_\mathrm{r}}{\mathrm{Vol}}$, $\frac{E_\mathrm{r}}{\mathrm{Mass}}$, or $\frac{E_\mathrm{r}}{\mathrm{Cost}}$ [29], [49]–[51], [56]–[63]; power density $\frac{P_\mathrm{r}}{\mathrm{Vol}}$ or $\frac{P_\mathrm{r}}{\mathrm{Mass}}$ [58], [64]; volumetric mass density or specific volume $\frac{\mathrm{Mass}}{\mathrm{Vol}}$ [4], [41]; and lifetime L_0 [31], [65].

Conventional *inductor* FOM satisfying the series-parallel modular invariance property includes the ac quality factor Q_ac [27], [66]–[71]; relative dissipation factor or relative loss factor $\frac{\tan\delta}{\mu_\mathrm{r}}$ [67], [72]; the volumetric core (eddy current or hysteresis) loss $\frac{P_\mathrm{loss}}{\mathrm{Vol}}$ [33], [68]; and the specific loss density $\frac{P_\mathrm{loss}}{\mathrm{Mass}}$ [73].

Because these capacitor and inductor FOM are suitable candidates for component comparison across the entire device subspace, future research explorations of these metrics could consider trade-offs and derive connections to the devices' broader system application [64].

D. Limited or Operating Condition Specific Capacitor Metrics

Some common-use device metrics, especially for capacitors, are only parallel modular and thus partially satisfy the series-parallel modular invariance property. These metrics can be utilized for device comparison, but require a more restrictive and judicious context, most commonly by only comparing capacitors of a specific rated voltage V_r. Some examples include current density $\frac{I_\mathrm{r}}{\mathrm{Vol}}$ and $\frac{I_\mathrm{r}}{\mathrm{Mass}}$ [48], [74]; capacitance-related current density $\frac{C}{I_\mathrm{r}}$ [74]; volumetric efficiency or charge density $\frac{C \cdot V_\mathrm{r}}{\mathrm{Vol}}$ [48]; capacitance density, volumetric capacitance, or capacitance volumetric efficiency $\frac{C}{\mathrm{Vol}}$ [31], [60], [75]–[77]; capacitance voltage product per rated current $\frac{C \cdot V_\mathrm{r}}{I_\mathrm{r}}$ [48]; cost per farad $\frac{\mathrm{Cost}}{C}$ [61]; and specific capacitance $\frac{C \cdot V_\mathrm{r}}{\mathrm{Mass}}$ [41], [43], [52].

E. Limitations of Series-Parallel Device Configurations

Arbitrarily configuring discrete components in series and in parallel has associated practical limitations: increased layout inductance, asymmetrical current distribution, unbalanced voltage distributions, and lower packing factor [60], [78], [79]. For the purposes of this FOM analysis, these shortcomings—which can be mitigated with conscientious design—are neglected.

III. COMMERCIAL CAPACITOR AND INDUCTOR DATA

Desired device FOM are constructed from base metrics, and thus the greater acquisition of base metrics directly enables the determination of more FOM. This section describes the availability and extent of the surveyed data for discrete commercial passive components. It also delineates the capacitor and inductor typologies used throughout this work.

A. Extent of Available Data – Capacitors

The present distributor data sets contain certain practicable information with varying degrees of consistency: (near) fully available, partially available, or not available. Satiating a partially or unavailable component attribute can enable the determination of secondary metrics (e.g., rated stored energy E_r and volume) and tertiary FOM (e.g., energy and power density). As discussed in Section II-A, this requires either supplemental measured data with extrapolation, or theoretic generalization of the component derived from material properties.

The comprehensive data set consists of an aggregation of roughly 606,000 distinct capacitors from the prominent distributor Digikey Electronics.

1) Fully Available Data: Readily available data includes several primary attributes: capacitor rated voltage V_r; the zero-voltage differential capacitance $C(0)$ [24]; the dimensional parameters: length, width, height, diameter; and the cost per unit. The secondary attribute 'box' or enclosure volume is computed from the dimensional attributes. For linear capacitors, the secondary attribute of rated stored energy E_r is calculable in aggregate from these base attributes. However, the prominent Class II ceramic capacitor technology has a nonlinear voltage-dependent capacitance characteristic [24], and thus E_r cannot

be calculated for all capacitor technologies without additional analysis presented in Section IV.

2) Partially Available Data: The equivalent series resistance (ESR); loss tangent or dissipation factor $\tan\delta = \mathrm{DF}$; rated rms current I_r; and lifetime L_0 are all critical attributes for any quantitative performance analysis of capacitor loss and reliability, however, these metrics are unavailable in the overall distributor data set for most capacitor technologies except for some aluminum electrolytic capacitors. Some of these base attributes also maintain a pertinent frequency and temperature dependence, and are inconsistently standardized across manufacturers. Thus even though correction factors are sometimes disclosed, the oftentimes singular values for ESR, $\tan\delta$, I_r, and L_0 common to catalogs and datasheets are often inadequate for involved electronics design.

To generalize and predict losses, some have collected sampled measurements for realistic, large-signal operating conditions and abstracted broad capacitor trends as a function of frequency, dc voltage bias, and temperature [3]. Others propose an empirical loss equation for capacitors [24]–[26], being the dual of the venerable Steinmetz equation for inductors [80], [81]. These models depend on the capacitor's excitation waveforms, and could directly integrate with a comprehensive component data set to generalize loss, however, this requires more extensive data sampling and more study.

3) Unavailable Data: Some primary attributes are essentially unavailable in the distributor data set. For instance, the component mass would be invaluable for quantitative evaluation of weight-optimized power conversion systems, however, presently this information is digitally available for only a select few suppliers. To reconcile the deficiency in mass data, Section V applies sampled measured data to estimate the mass of all capacitor components as a function of its type, rated voltage V_r, and capacitance C.

B. Surveyed Technologies – Capacitors

Commercially viable capacitors are constructed in a variety of technologies best suited for particular electrical applications [48], [82]. Technologies are most easily distinguished by the dielectric material where certain capacitor types excel in cost, reliability, high-frequency capability, voltage and current ratings, mass, and volume. In this work, the capacitors in the comprehensive data set are classified into subsets with distinct elements: aluminum electrolytic, tantalum electrolytic, Class I and Class II ceramic, film, and electrolytic double-layer. The work in [83] clarifies the precise distinctions between these capacitor technologies as applied in this work. Fig. 2 illustrates, for the surveyed data, a conventional differentiator between capacitor technologies: the range of possible capacitance C and rated dc voltage V_r.

Niobium electrolytic, mica, and silicon capacitors are other notable capacitor technologies. However for these types, the quantity of commercial devices is small and the relevant data is sparse, thus, they are not considered in greater detail within this work.

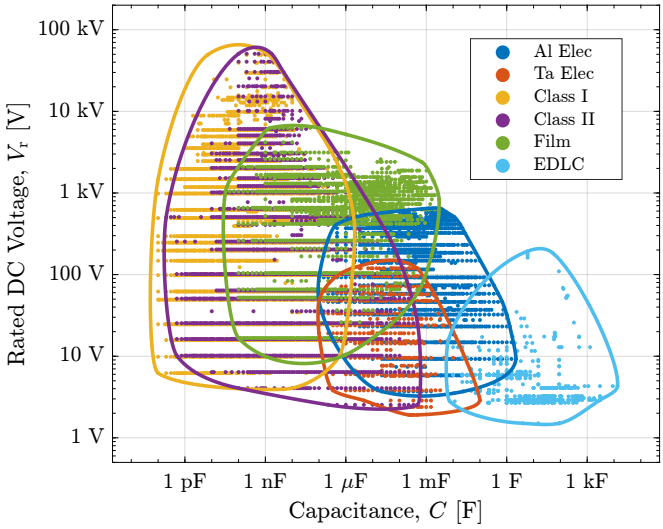

Fig. 2. Survey of component rated capacitance C versus rated dc voltage V_r across all major capacitor technologies including aluminum electrolytic, tantalum electrolytic, Class 1 ceramic, Class II ceramic, film, and electrolytic double-layer capacitors (EDLC).

C. Extent of Available Data – Inductors

Similar to capacitor components, the base attributes for inductors have varying degrees of availability in the comprehensive data set. Data on roughly 88,000 distinct inductors were aggregated in total from the distributor Digikey Electronics.

1) Fully Available Data: Readily available data includes several primary attributes: inductance at zero bias current L; inductor thermal rated rms current I_rms (conventionally at a $40\,^\circ\mathrm{C}$ increase in temperature); peak saturation current limit I_sat (often defined at either 20% or 40% inductance derating); the dc resistance DCR; the dimensional parameters: length, width, height, diameter; and the cost per unit. The 'box' volume and the rated stored energy E_r are calculable in aggregate from these base attributes.

2) Partially Available Data: The ac quality factor $Q_\mathrm{ac} = \frac{2\pi f L}{R_\mathrm{ac}}$ FOM quantifies the ideality and damping of the inductor and predicts losses [66]. Manufacturers measure and report Q_ac for a small-signal excitation at a singular test frequency f, however, this attribute is only partially available (roughly 60% of aggregated inductors) in the comprehensive data set. Additionally, roughly 20% of surveyed inductors have undefined or poorly defined core material; these were discarded from the analysis.

3) Unavailable Data: As with capacitors, the component mass of inductors is largely absent from the comprehensive data set. In Section V, sampled measured data is used to estimate the mass of all inductor components as a function of its type, rated current I_r, and inductance L.

D. Surveyed Technologies – Inductors

Analogous to capacitors, inductors are most distinguishable by the type of core material: ferrite, metal, or non-magnetic/air. The core material significantly impacts suitable operating frequency ranges, core losses, and saturation limits for magnetic flux. Again, the work in [83] clarifies the precise distinctions

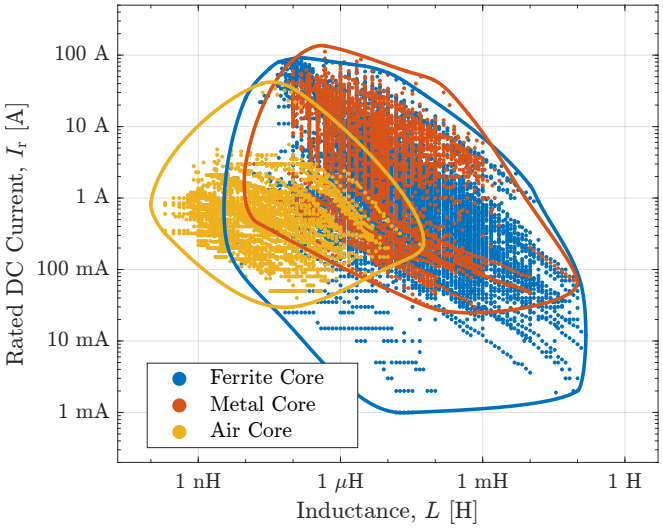

Fig. 3. Survey of component rated inductance L versus rated dc current I_r across all major inductor technologies including ferrite core, metal (including powdered) core, and air core.

between these inductor technologies as applied in this work. Fig. 3 illustrates the inductance L and rated current I_r for each commercial inductor technology.

IV. Sampled Data and Extrapolation: Stored Energy of Class II Ceramic Capacitors

Class II ceramic capacitors are a unique component type that requires special consideration in data analysis. Their significant voltage, temperature, and age dependence makes the determination of certain metrics circuitous compared to stable capacitor technologies. However, Class II multilayer ceramic chip (MLCC) capacitors are a particularly good capacitor choice for electronics due to their comparatively low losses, high energy density, and widespread applicability [3], [25]. A discussion of the best capacitor technologies is markedly incomplete without the inclusion of this capacitor type, thus intentional effort is exerted to determine their rated stored energy E_r and compute energy density FOM γ.

In this section, an empirically derived fit is shown to accurately estimate the voltage-dependent stored-energy-equivalent capacitance $C_E(v)$ at any dc voltage v, specifically at the rated dc voltage $v = V_r$. This fit only depends on the differential capacitance $C(v)$ known at two values: $v = 0\,\mathrm{V}$ and $v = V_r$. The approximation is validated by using datasheet information from a sampling of 2,550 MLCC capacitors manufactured by the TDK Corporation.

A. Standards

Class II ceramic capacitors are primarily distinguished by an associated alphanumeric code indicating some information about the temperature characteristic (TC) or temperature-voltage characteristic (TVC). There are three primary standards codifying these nonlinear characteristics:

1) EIA RS-198: the most common in use (e.g., X6S, Y5V, C0G) but only specifies TC information [84].
2) IEC/EN 60384-1: less commonly used (e.g., NP0, 2X1) and specifies information about TC and TVC [85].
3) MIL-C-11015: military standard which specifies TVC information [86].

For all standards, codes indicate information about temperature range, expected capacitance derating at these temperature limits, and expected capacitance derating at rated voltage. Unfortunately, when using the prominent EIA standard, any two capacitors with the same code (e.g., X6S) and thus similar TC do not necessarily have similar or even necessarily correlated TVC [24].

B. Defining Capacitance and Stored Energy

Regardless of the TC or TVC, a coherent definition of energy storage for nonlinear capacitors is necessary to eventually deduce energy-related FOM. For a general capacitor, the stored energy E is completely defined at an applied dc voltage V_a as

$$E_a = E(V_a) := \int_{q(0)}^{q(V_a)} v\,\mathrm{d}q = \int_0^{V_a} v\,C(v)\,\mathrm{d}v \tag{1}$$

where $C(v)$ is the characteristic incremental, small-signal, or differential capacitance [24], [25], [87], [88] defined as

$$C(v) := \frac{i}{\left(\frac{\mathrm{d}v}{\mathrm{d}t}\right)} = \frac{\mathrm{d}q}{\mathrm{d}v}. \tag{2}$$

For a linear capacitor, the differential capacitance C is constant with applied voltage (and temperature). Thus by evaluating (1), the integral equation for stored energy at an applied dc voltage V_a simplifies to

$$E_{a,\mathrm{linear}} = \frac{1}{2}CV_a^2 \tag{3}$$

which is notably invalid for voltage-dependent capacitors:

$$E_{a,\mathrm{nonlinear}} \neq \frac{1}{2}C(V_a)V_a^2. \tag{4}$$

since the $C(v)$ varies with voltage.

The stored energy E_a of a nonlinear capacitance at an applied voltage V_a can instead be equivalently defined using an effective energy-equivalent capacitance C_E at V_a

$$E_a = \frac{1}{2}C_E(V_a)V_a^2. \tag{5}$$

Equating (1) and (5), the energy-equivalent capacitance $C_E(v)$ [87] can be computed as a function of the differential capacitance curve $C(v)$:

$$C_E(V_a) = \frac{2E_a}{V_a^2} = \frac{2}{V_a^2}\int_0^{V_a} v\,C(v)\,\mathrm{d}v. \tag{6}$$

For linear capacitors with voltage-invariant capacitance C, the energy-equivalent capacitance reduces simply to $C_E = C$.

C. Data Acquisition

Within the context of programmatic data acquisition, there are varying degrees of information available that can help determine the energy-equivalent capacitance $C_E(V_r)$, and thus rated stored energy E_r and energy density γ.

- $C_0 = C(0)$ – The zero-voltage differential capacitance

- V_r – Rated dc voltage
- TC – Temperature characteristic code
- TVC – Temperature-voltage characteristic code
- $C(v)$ – Characteristic C-V curve (differential capacitance)
- $C_\mathrm{r} = C(V_\mathrm{r})$ – Differential capacitance at rated voltage

The first three attributes: C_0, V_r, and TC code, are defining characteristics of every capacitor and are readily available in the comprehensive distributor data set. The full $C(v)$ curve as well as differential capacitance C_r at rated voltage are not directly available from distributors, however they are often available on datasheets. The TVC code is rarely available anywhere, including datasheets.

The TDK Corporation, a prominent capacitor manufacturer, publicly provides digitized differential capacitance $C(v)$ data for their Class II MLCC components in conjunction with C_0, V_r, and TC. Although not a sufficiently comprehensive survey of all Class II ceramics, a sampling of roughly 2,550 TDK Class II MLCC components informs several meaningful insights for the Class II ceramic capacitor technology as a whole.

D. Stored Energy Approximation: Using Temp. Characteristic

It would be convenient to approximate rated energy E_r in (1) or the rated energy-equivalent capacitance $C_\mathrm{E}(V_\mathrm{r})$ in (6) without express requirement of the entire $C(v)$ characteristic curve which cannot presently be attained en masse. One potential method is to identify general trends in the $C(v)$ curves of capacitors with specific temperature characteristics (e.g., X6S, X7R). For instance, X6S capacitors could have an approximate 70-90% capacitance derating at V_r, whereas X5R capacitors could have an approximate 60-70% capacitance derating. Such an identifiable relationship would aid estimation of E_r with sparse information. Prior work has investigated the existence of a practicable linkage between TC and capacitance-voltage dependence [89], [90].

The relative shapes and values of the $C(v)$ curves are aggregately visualized in Fig. 4 to identify patterned correlations with the TC and determine whether a TC-dependent scheme has plausible utility. All C-V curves are normalized as $C(v)/C(0)$, and the differential capacitances generally derate with a characteristic logistic or mirrored 'S' shape (for a log-linear plot). Visual inspection yields some groupings or families of $C(v)$ curves for similar TC indicating similar dielectric materials, however they are not visibly distinctive enough to determine any generalized correlations between TC and $C(v)$; consequently, a different method must be employed to approximate E_r.

E. Stored Energy Approximation: Using $C(0)$ and $C(V_a)$

The effective energy-equivalent capacitance $C_\mathrm{E}(V_\mathrm{a})$ at applied voltage V_a could possibly be estimated knowing only at most two values: $C(0)$ and $C(V_\mathrm{a})$. Different approximations of $C_\mathrm{E}(V_\mathrm{a})$ are presented and evaluated compared to the exact value in (6).

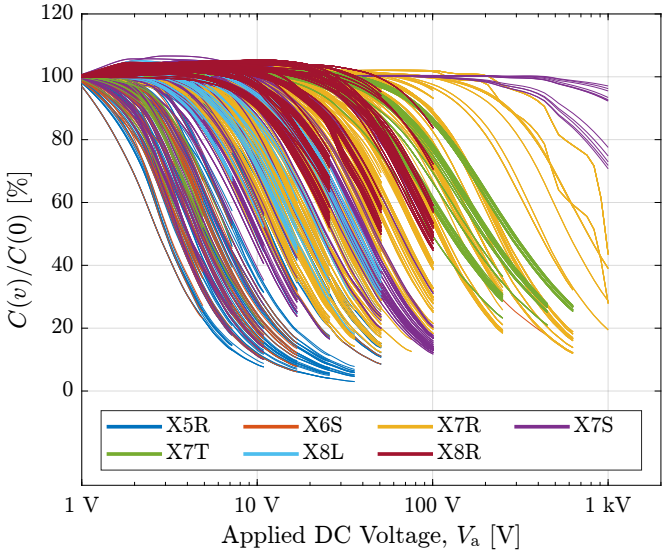

Fig. 4. Applied dc voltage V_a versus normalized differential capacitance $C(v)/C(0)$ and distinguished by temperature characteristic. Data is sampling of 2,550 TDK Class II MLCC capacitors.

TABLE II
PERCENTAGE ERROR FOR $C_\mathrm{E}(V_\mathrm{r})$ APPROXIMATIONS

$C_\mathrm{E}(V_\mathrm{r})$	$C(0)$	$C(V_\mathrm{r})$	$\frac{2}{3}C(V_\mathrm{r}) + \frac{1}{3}C(0)$	$M_{-0.5}(C(0), C(V_\mathrm{r}))$
Mean	98.8%	32.4%	16.0%	3.1%
Median	64.3%	33.9%	5.2%	1.8%

1) Zeroth-order approximation: Most simply, the energy-equivalent capacitance C_E at an applied voltage V_a can be approximated evaluating $C(v)$ at its limits as

$$C_\mathrm{E}(V_\mathrm{a}) \approx C(0) \tag{7}$$

or as

$$C_\mathrm{E}(V_\mathrm{a}) \approx C(V_\mathrm{a}). \tag{8}$$

These estimates roughly serve as upper and lower bounds, respectively, on the actual $C_\mathrm{E}(V_\mathrm{a})$.

2) First-order approximation: For this approximation of $C_\mathrm{E}(v)$ the differential capacitance $C(v)$ is approximated by a linear fit, or first-order approximation, between the zero-voltage capacitance $C(0)$ and the differential capacitance at the applied voltage $C(V_\mathrm{a})$.

$$C(v) \approx \frac{C(V_\mathrm{a}) - C(0)}{V_\mathrm{a} - 0} v + C(0) \tag{9}$$

Directly evaluating (6) using (9) yields

$$C_\mathrm{E}(V_\mathrm{a}) \approx \frac{2}{3}C(V_\mathrm{a}) + \frac{1}{3}C(0). \tag{10}$$

3) Power mean approximation: Finally, $C_\mathrm{E}(V_\mathrm{a})$ is approximated with a special average function. The power mean (or Hölder mean) M_p is a family of functions which averages n positive numbers $x_1, x_2, ..., x_n$ as

$$M_p\left(x_1, x_2, ..., x_n\right) := \left(\frac{x_1^p + x_2^p + ... + x_n^p}{n}\right)^{\frac{1}{p}} \tag{11}$$

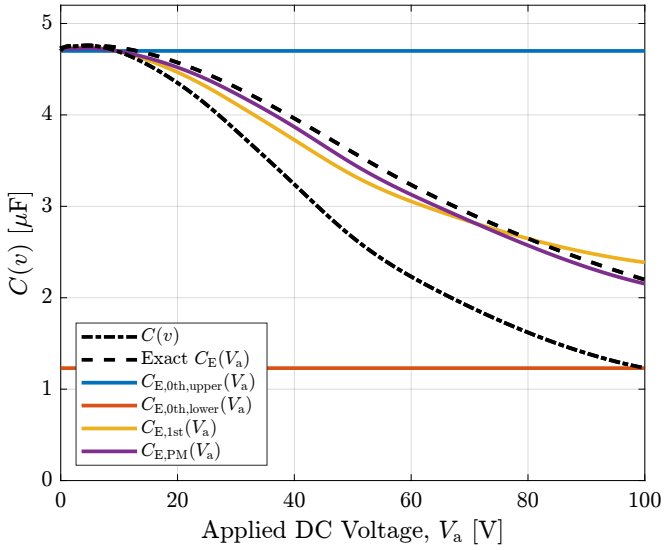

Fig. 5. Applied dc voltage versus differential capacitance $C(v)$ for device C5750X7R2A475K230KA: $C(0) = 4.7\,\mu$F, $V_r = 100$ V, X7R. Demonstrates comparison of approximations for energy-equivalent capacitance $C_E(V_a)$.

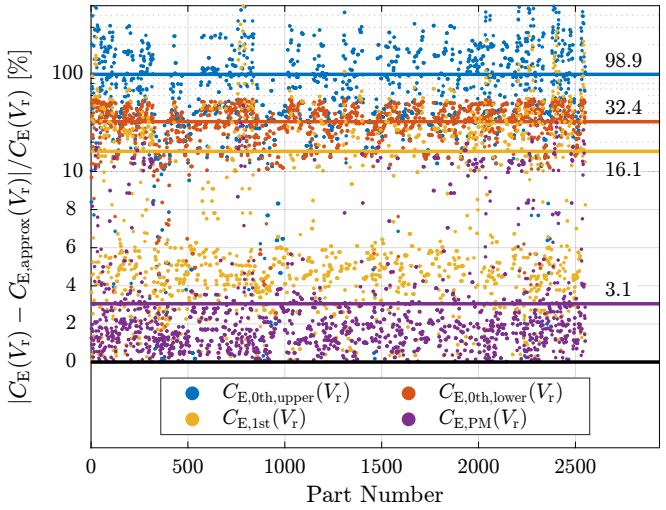

Fig. 6. Percentage error for approximations of energy-equivalent capacitance $C_E(V_r)$ at rated dc voltage V_r. Solid horizontal lines indicate the mean percentage error for each corresponding approximation. Data is sampling of 2,550 TDK Class II MLCC capacitors.

where the exponent p is some real nonzero number [91], [92]. This power mean is equivalent to other well-known means for particular values of p: the arithmetic mean for $p = 1$, the quadratic mean or root mean square (RMS) for $p = 2$, and the harmonic mean for $p = -1$; it is also related to the ℓ^p-norm of a vector for integer $p \geq 1$ [93].

A good value of p results in the best approximation of $C_E(V_a)$ at every applied dc voltage $0 < V_a < V_r$ utilizing only the endpoints of the differential capacitance curve $C(0)$ and $C(V_a)$ or as $C_E(V_a) \approx M_p(C(0), C(V_a))$. Using (6), the energy-equivalent capacitances at rated voltage $C_E(V_r)$ are computed for all 2,550 sampled Class II MLCC capacitors from TDK. Then regression is applied to fit this data to (11) yielding a best fit value $p = -0.504 \approx -0.5$ and an empirically derived approximation

$$C_E(V_a) \approx M_{-0.5}\big(C(0), C(V_a)\big) = \frac{4C(0)C(V_a)}{\Big(\sqrt{C(0)} + \sqrt{C(V_a)}\Big)^2}. \tag{12}$$

4) Results: All $C_E(v)$ approximations are graphically compared for a particular device in Fig. 5 across applied voltage V_a. From inspection, the proposed first-order and power mean approximations in (10) and (12) very nearly match the general waveshape of the actual $C_E(v)$ curve evaluated from (6).

To prove their efficacy, these estimates must also be validated for the entire sampled data set—not just a single component. The relative accuracy of an estimate is judged by its mean percentage error

$$\text{MPE} = \frac{1}{N}\sum_{i=1}^{N} \frac{|x_{\text{actual},i} - x_{\text{predicted},i}|}{x_{\text{actual},i}} \tag{13}$$

for N elements in a set where $x = C_E(V_r)$. Fig. 6 presents the percentage error of each $C_E(v)$ approximation for all 2,550 sampled TDK components; the resulting mean and median percentage error of each approximation are tabulated in Table II. The zeroth-order approximations (7) and (8) result in prohibitively high estimation inaccuracy, but the power mean approximation in (12) has a low MPE of 3.1% (median percentage error of 1.8%), sufficiently validating its usage amongst the others.

This method suggests if ever a manufacturer, supplier, or distributor reports the differential capacitance values of Class II ceramic capacitors at both zero dc voltage bias $C(0)$ and at rated dc voltage bias $C(V_r)$, then the rated stored energy E_r, and consequently energy densities γ, at rated voltage V_r could be estimated with a relatively high degree of accuracy using (12) without requiring the full $C(v)$ curve, temperature characteristic, or temperature-voltage characteristic.

F. Investigating Energy Density FOM of Sampled Data

The FOM framework proposed in Secion II can be applied to the sampled TDK data set. The exact rated stored energy E_r, as well as the volumetric energy density $\gamma_v = \frac{E_r}{\text{Vol}}$, of each capacitor is computed as (1). Recall that the series-parallel modularity invariance property of a FOM allows every capacitor, regardless of rated voltage, to be fairly compared.

Fig. 7 shows the consequent impact of TC and energy-equivalent capacitance $C_E(V_r)$ approximation on γ_v with respect to rated voltage V_r. Despite some TC clustering, the relationship between TC and γ_v in Fig. 7a is not correlative enough to predict a TC code that has the smallest volume nor the γ_v of any individual capacitor based on its TC. The associated Pareto fronts for each approximation method are also included relative to the exact Pareto front of volumetric energy density γ_v in Fig. 7b. If using the simplest zeroth-order approximation in (7), the highest energy density capability of Class II ceramic capacitors can be overestimated by as much as 1000×. The recommended power approximation in (12) sufficiently estimates γ_v.

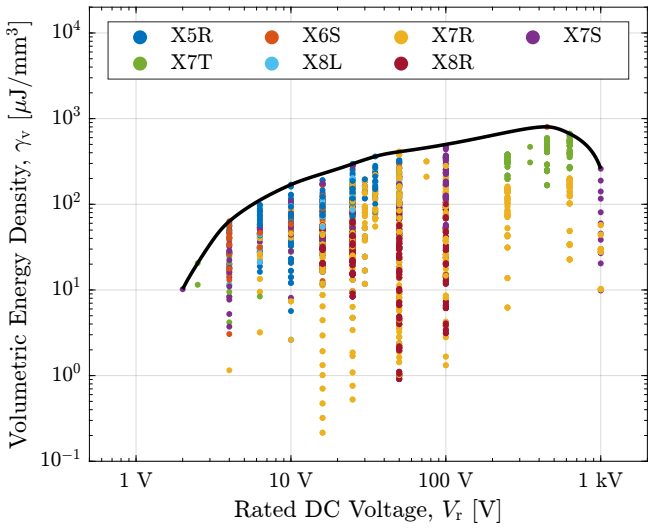

(a)

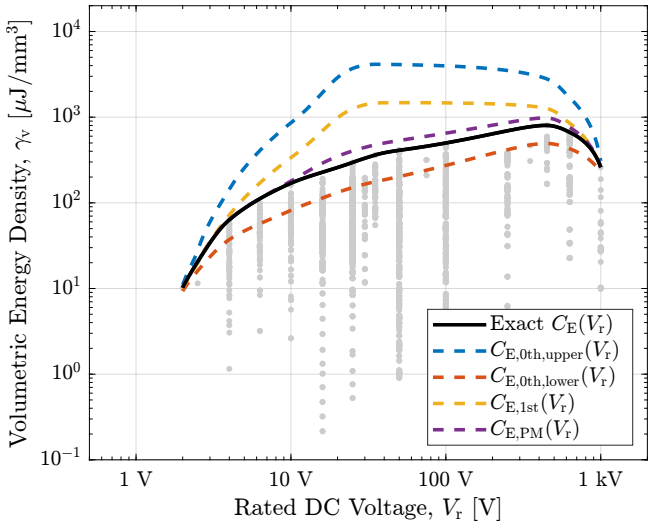

(b)

Fig. 7. Rated dc voltage V_r versus volumetric energy density γ_v for TDK Class II MLCC capacitors where (a) components are delineated by temperature characteristics and (b) the Pareto front varies depending on the approximation for $C_E(V_r)$.

G. Extrapolating Sampled Data to the Full Data Set

This analysis concludes that energy storage estimation of Class II ceramic capacitors is possible if the differential capacitance at two voltages, 0 V and V_a, are known. However, as previously mentioned, the comprehensive data set only contains $C(0)$ data for all capacitors. Thus for the remainder of this work, the energy equivalent capacitance $C_E(V_r)$ at rated voltage is uniformly approximated as 60 % of $C(0)$—an improvement over the zeroth-order estimate of in (7)—to estimate the rated energy storage E_r of Class II ceramic capacitors. This approximation has a mean percentage error MPE of 40% applied to the TDK data set. This is an inaccurate and dissatisfying estimate, but reasonable considering the logarithmically wide breadth in energy densities across the technology as shown in Fig. 7. If capacitor manufacturers, suppliers, and distributors begin to report values for $C(V_r)$—doubly useful because it conveys small-signal capacitance at rated voltage—then $C_E(V_r)$ can be estimated with a high degree of accuracy using the power mean in (12), fully enabling estimation of rated energy storage E_r for all capacitors, both linear and nonlinear, and satisfyingly quantifying those device FOM related to energy.

H. Application to Nonlinear Inductors

Analogous to Class II ceramic capacitors, ferrite and metal core inductors have a non-uniform differential inductance $L(i)$ dependent on the applied current i. Consequently, the peak energy density of inductors reported in this work (see Fig. 11, Fig. 13, and Fig. 14) utilizes an approximation for energy-equivalent inductance L_E similar to the zeroth-order approximation for energy-equivalent capacitance (8). Calculable exact peak energy storage at rated current I_r—or even more accurate estimation—is not possible without a sufficiently large sampled data set of $L(i)$ curves; unfortunately, no present manufacturers have digitized $L(i)$ curves available en masse.

V. Sampled Data and Extrapolation: Capacitor and Inductor Mass

Although minimized volume and cost are often desired, minimizing the system mass can also be a critical need for electronics applications. In particular, innovations in the mass reduction for mobile electronics—most commonly electric aircraft or automobiles—are driven by sustainable energy targets for the growing electric propulsion industry [94], [95]. Electronics for space applications also prioritize lightweight designs. In these applications, even the choice of converter topology is informed by the achievable mass of the system and the requisite masses of the constituent devices [96]–[99]. The mass of commercially available capacitors and inductors remains largely indeterminable en masse as few manufacturers supply this information. Thus, an insufficient proportion of component mass is known for the comprehensive data set surveyed in this work.

This section expands on the analysis introduced in [4]. Determining the volumetric mass density (mass per volume) D of a broadly sampled set of passive devices through measurement yields sufficient information to extrapolate and transform readily available volume data to an estimated value of mass for each component. This work presents generic fits for both capacitor and inductor density D, with relevant empirical parameters provided for all major capacitor and inductor technologies as described in Section III.

A. FOM Transformation – Theory

The volumetric mass density (or density) of any component

$$D = \frac{\text{Mass}}{\text{Vol}} \tag{14}$$

is an intrinsic FOM relating its mass to its volume. Incidentally, the density D (as well as mass) for every component in the comprehensive data set is unknown. However, a single estimated value of D may apply to an entire component technology by relying on homogeneity in material composition and construction. This value of D can be further refined

TABLE III
RESULTS OF PROPOSED MEAN FIT AND EMPIRICAL POWER FIT FOR CAPACITOR/INDUCTOR VOLUMETRIC MASS DENSITY (MASS/VOLUME). PARENTHESIS INDICATE BOUNDS OF 95% CONFIDENCE INTERVAL FOR RELEVANT PARAMETERS.

Component Technology	Quantity	Mean Fit		Power Fit				
		$D\left[\frac{\text{mg}}{\text{mm}^3}\right]$	**MPE**	k	α	β	p-value	**MPE**
Al Electrolytic	47	1.49 (±0.55)	**9.16%**	1.52 (1.29, 1.80)	−0.0710 (±0.0332)	−0.0257 (±0.0193)	4.29e-04	**7.80%**
Ta Electrolytic	64	3.38 (±0.12)	**12.87%**	4.93 (4.24, 5.73)	0.0482 (±0.0447)	0.0498 (±0.0152)	4.40e-08	**8.49%**
Class I Ceramic	46	4.39 (±0.24)	**13.97%**	11.66 (8.17, 16.64)	0.0558 (±0.0426)	0.0665 (±0.0165)	1.02e-09	**10.0%**
Class II Ceramic	66	5.41 (±0.17)	**10.17%**	8.41 (6.80, 10.40)	−0.0045 (±0.0311)	0.0272 (±0.0130)	1.29e-04	**8.46%**
Film	92	1.26 (±0.02)	**7.70%**	1.15 (0.98, 1.35)	−0.0411 (±0.0199)	−0.0222 (±0.0079)	1.44e-08	**5.98%**
Ferrite Core	34	3.12 (±0.25)	**21.03%**	2.39 (1.36, 4.19)	−0.0466 (±0.0856)	−0.0280 (±0.0568)	0.5029	**19.86%**
Metal Core	87	5.04 (±0.14)	**11.90%**	7.33 (5.66, 9.49)	0.0903 (±0.0215)	0.0464 (±0.0203)	4.83e-14	**7.71%**
Air Core	11	1.45 (±0.27)	**25.45%**	1.95 (0.13, 30.3)	0.1659 (±0.1232)	0.0453 (±0.1874)	0.0250	**14.40%**

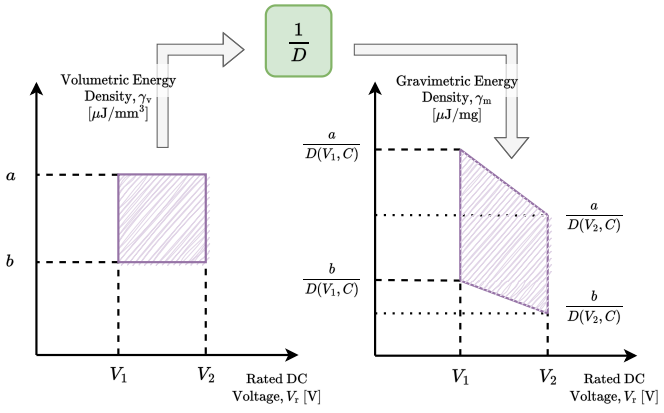

Fig. 8. Portrayal mapping capacitor volumetric energy density γ_{v} to gravimetric energy density γ_{m} using a density transformation $D(V_{\text{r}}, C)$ dependent on rated dc voltage V_{r} and capacitance C.

by empirically fitting its dependence to known component attributes: the capacitance C and rated dc voltage V_{r} for capacitors, and inductance L and rated dc current I_{r} for inductors.

Once a reliably accurate density mapping D is known, then a volume-related FOM for an individual component can be transformed into a mass-related FOM as

$$\gamma_{\text{m}} = \frac{1}{D}\,\gamma_{\text{v}}. \tag{15}$$

The volumetric energy density FOM γ_{v} for each passive component is defined as a ratio of rated energy E_{r} and volume:

$$\gamma_{\text{v}} = \frac{E_{\text{r}}}{\text{Vol}} \tag{16}$$

whereas the gravimetric energy density FOM γ_{m} is defined as a ratio of rated energy E_{r} and mass:

$$\gamma_{\text{m}} = \frac{E_{\text{r}}}{\text{Mass}}. \tag{17}$$

The rated stored energy metric E_{r} is computed for capacitors from the energy-equivalent capacitance C_{E} in (6) and rated dc voltage V_{r}

$$E_{\text{r}} = \frac{1}{2} C_{\text{E}}(V_{\text{r}}) V_{\text{r}}^2 \tag{18}$$

and is computed for inductors from the inductance L and rated dc current I_{r}

$$E_{\text{r}} = \frac{1}{2} L I_{\text{r}}^2. \tag{19}$$

The inductor's rated dc current I_{r} is defined as the minimum of the thermal rms current rating I_{rms} and the peak saturation current rating I_{sat} as specified on the datasheet, or

$$I_{\text{r}} = \min(I_{\text{rms}}, I_{\text{sat}}). \tag{20}$$

Fig. 8 illustrates this transformation principal in (15) by mapping a set of capacitor volumetric energy density data γ_{v} to a set of gravimetric energy density data γ_{m} utilizing a density D that is dependent on C and V_{r}.

B. Volumetric Mass Density Measurement

The mass and box volume of 315 unique capacitors and 132 unique inductors were measured to construct empirical estimates for the density D. To capture a sufficiently diverse spread of device variants, capacitors were selected to encompass a vast range of package sizes, rated dc voltages V_{r}, capacitance C, and manufacturer. Inductors were similarly selected to encompass a breadth of package sizes, rated current I_{r}, inductance L, and manufacturer. For each unique component, multiple samples were weighed based on the accuracy of the electronic scale to limit the relative measurement error to a maximum of 0.5%. Fig. 9 shows the measured density D as a function of C and V_{r} for each capacitor in Fig. 9a and as a function of L and I_{r} for each inductor in Fig. 9b.

C. Empirically Fitting Density Measurements

Two empirically derived fits are proposed by utilizing the measured density data: 1) a mean or constant fit and 2) a power fit dependent on base electrical attributes.

1) Mean Fit Estimate: Passive components are separated by type, then a mean fit for density D is calculated for each with a zeroth-order linear regression. These mean densities are indicated in Table III along with their 95% confidence intervals assuming a normal distribution of the measured data. By ranking of least to most dense, the component technologies are ordered as film capacitor, air core inductor, aluminum electrolytic capacitor, ferrite core inductor, tantalum

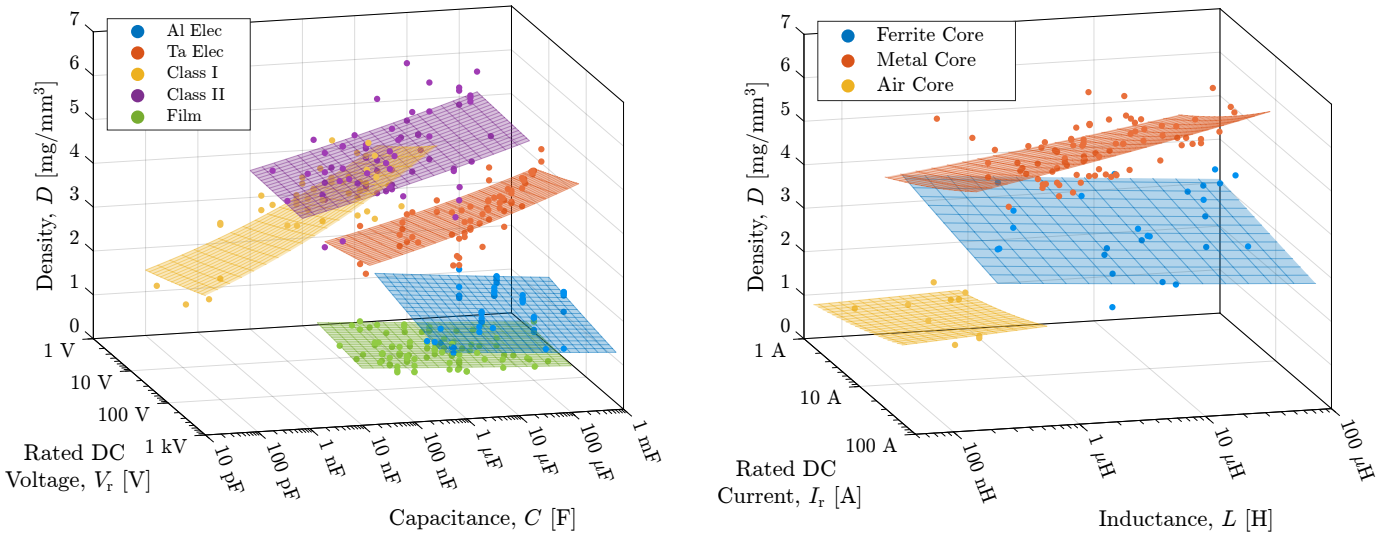

Fig. 9. Measured volumetric mass density D for (a) capacitors as a function of rated dc voltage V_r and capacitance C and (b) inductors as a function of rated dc current I_r and inductance L. A best power fit surface in (21) and (22) is visualized for each component technology: (a) aluminum electrolytic, tantalum electrolytic, Class I ceramic, Class II ceramic capacitors film capacitors; (b) ferrite, metal, and air core inductors.

electrolytic capacitor, Class I ceramic capacitor, metal core inductor, and Class II ceramic capacitor.

The relative accuracy of a fit is judged by its mean percentage error MPE defined in (13) where x is the density D. The computed MPE is less than 30% for every mean fit tabulated in Table III, indicating a fairly accurate fit between the measured and the mean fit approximation. The MPE can be further reduced by utilizing a more accurate power fit model dependent on base component attributes (e.g., C, V_r, L, I_r) fully available in the comprehensive data set as described in Section III.

2) Power Fit Estimate: A possible correlation between density D and rated dc voltage V_r and capacitance C (for capacitors) emerges from inspection of the measured densities in Fig. 9. Taking inspiration from classical empirical fits for loss in passive components [25], [81] while remaining conscientious of statistical uncertainty in inferential models [100], this work proposes a power fit expression for density D as

$$D = k \cdot V_r^{\alpha} \cdot C^{\beta} \quad \left[\frac{\text{mg}}{\text{mm}^3}\right] \tag{21}$$

with inputs V_r and C, and empirical parameters k, α, and β. An analagous power fit expression is proposed for inductors

$$D = k \cdot I_r^{\alpha} \cdot L^{\beta} \quad \left[\frac{\text{mg}}{\text{mm}^3}\right] \tag{22}$$

with inputs rated dc current I_r and inductance L, and similar empirical parameters k, α, and β.

Linear regression, applied to the logarithm of (21) and (22), is used to determine the best fit parameters k, α, and β which minimize the MPE [101]. Table III tabulates the resultant fit parameters (including the 95% confidence interval of each in parenthesis) of the power fit for each component technology as well as the associated statistical p-values and mean percentage error MPE

The p-value indicates the occurrence probability of the best-fit parameters when assuming the null hypothesis—in this case, a constant fit D with $\alpha = 0$ and $\beta = 0$—to be true. All statistical p-values—except for ferrite and air core inductors—are much lower than a typical significance threshold of 0.05, confirming the modeled power fits, with the specified parameters, are statistically significant [102].

Observing the empirical fit results, the densities of some capacitor technologies have a positive correlation with rated voltage V_r (e.g., tantalum electrolytic, Class I ceramic, and film), while some have a negative correlation (e.g., aluminum electrolytic). Empirical trends also exist with respect to the capacitance C: positive correlation for tantalum electrolytic, Class I ceramic, Class II ceramic, and film; and negative correlation for aluminum electrolytic. Similarly, metal core and air core inductor density correlates with respect to either rated dc current I_r or inductance L. The fit for ferrite core inductors insufficiently describes the density of the measured data; this likely results from wide variability in the constructions of this inductor type as well as high variance in the fill factor of the box volume used for the density calculation. In general, the typical intrinsic materials and construction for each component technology cause these parametric dependencies in capacitance C, voltage V_r, inductance L, or current I_r. These correlations produce interesting implications for present and future innovations in material science and packaging, however, this work does not explore these implications further and merely suggests perceived trends from phenomenological observation of the measured data.

3) Comparison Between Fits: The power fit estimation further reduces the prediction error compared to mean fit estimation. As a result, designers can either utilize the mean fit estimation to quickly predict a component's density D, and thus its mass and gravimetric energy density γ_m, or utilize the power fit estimation to improve predictive accuracy without

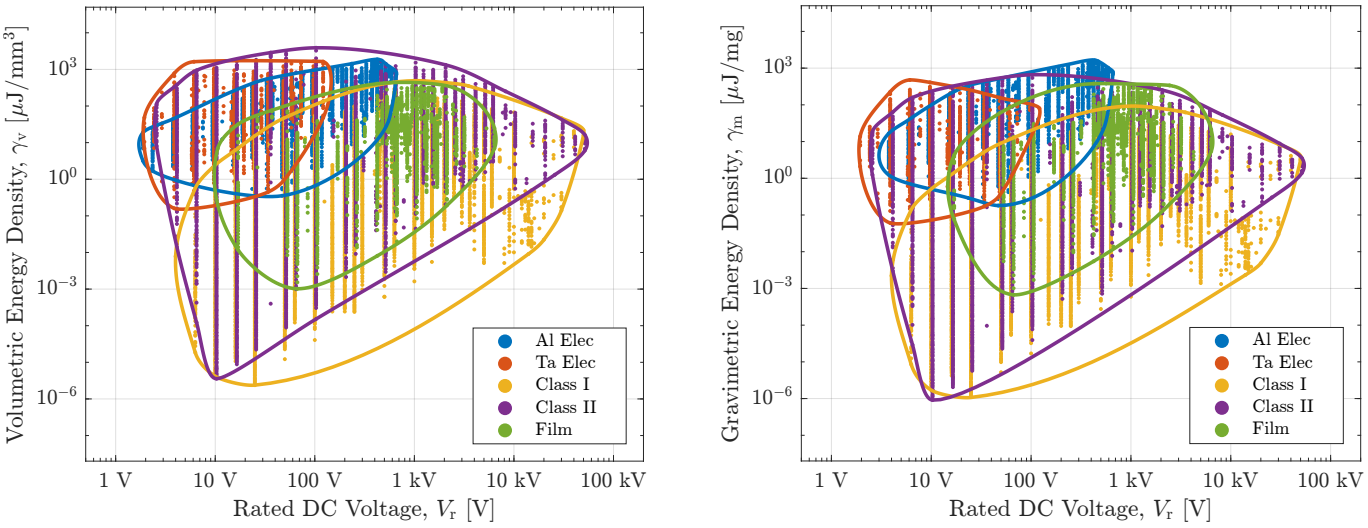

(a) Volumetric energy density γ_v

(b) Gravimetric energy density γ_m

Fig. 10. Energy density FOM of commercial capacitors across common technologies. The density $D = \frac{\text{Mass}}{\text{Vol}}$ of each capacitor in the comprehensive data set is empirically estimated with the power fit described in (21) and parameters in Table III. The gravimetric energy density γ_m is then computed by transforming the volumetric energy density γ_v in (15). The resulting transformation is subtle, yet significant at the highest energy densities.

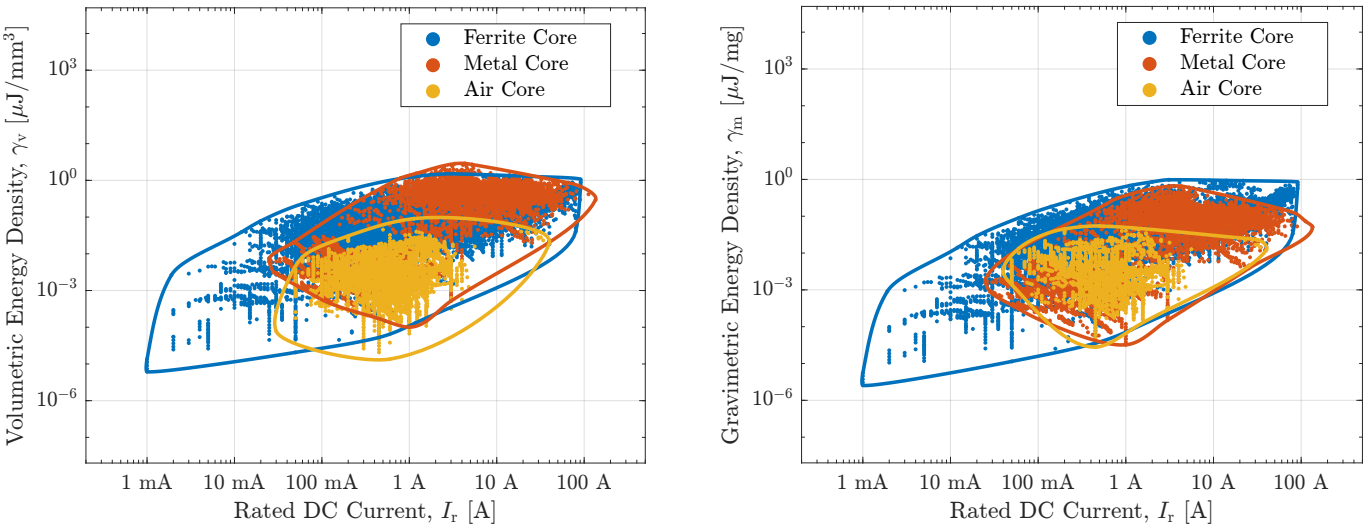

(a) Volumetric energy density γ_v

(b) Gravimetric energy density γ_m

Fig. 11. Energy density FOM of commercial inductors across common technologies. The density $D = \frac{\text{Mass}}{\text{Vol}}$ of each inductor in the comprehensive data set is empirically estimated with the power fit described in (22) and parameters in Table III. The gravimetric energy density γ_m is then computed by transforming the volumetric energy density γ_v in (15). The resulting transformation is subtle, yet significant at the highest energy densities.

much added inconvenience.

D. FOM Transformation – Application

Now buttressed with substantive estimates for component density D, the transformation theory introduced in Section V-A is applied to extrapolate box volume to mass for the comprehensive passive component data set introduced in Section III.

The visualization in Fig. 10 applies the FOM transformation in (15) and Fig. 8 to the comprehensive data set by utilizing the power fit expression for density D in (21) and (22) with best fit empirical parameters in Table III. In Fig. 10a, the rated dc voltage V_r versus volumetric energy density γ_v of every commercially surveyed capacitor is distinguished by technology. Fig. 10b depicts the gravimetric energy density γ_m, after applying the capacitance and voltage-dependent estimation for $D(V_r, C)$. After the density transformation, the shape of each component technology set marginally distorts and the sets shift relative to each other.

An analogous volume-to-mass transformation is performed for the commercial inductors in the comprehensive data set. The volumetric energy density γ_v in Fig. 11a maps to gravimetric energy density γ_m in Fig. 11b with the inductance and current-dependent power fit estimation for density $D(I_r, L)$ in (22).

With the analysis proposed in this section, all device FOM comprised of mass can be estimated to a high degree of accuracy using the expressions in (21) and (22) with empirically derived parameters in Table III, fully enabling estimation of mass for all capacitors and inductors. The energy density FOM of the comprehensive data is more deeply investigated in Section VI.

VI. Analyzing the Data

The comprehensive data set of commercial passive components has been clearly defined and its energy and mass deficiencies bolstered in Section IV and Section V, respectively. With this foundation set and a utilitarian FOM framework established, the data can be freely interpreted and analyzed. It is possible to infer fundamental limitations intrinsic to a component technology as well as quantified comparisons between technologies, even between capacitors and inductors. The prototypical question posed in Section II ("Based on the present available technology, the smallest possible capacitor solution for this application has volume X.") now has a determinable answer. From Fig. 10a, Class II ceramic capacitors are the capacitor technology with the smallest volume (with respect to energy storage), since they have the highest volumetric energy density. Similar quantifiably supported claims will be made throughout this section, including application to optimally choosing capacitors (or inductors) with an overrated voltage (or current).

A. Capacitor Voltage Overrating

For an applied capacitor voltage V_a, selecting a capacitor with a greater rated voltage V_r—called 'voltage overrating'—is often necessary depending on temperature and lifetime requirements [103] but, interestingly, can also be worthwhile to improve the realized capacitor volume, mass, or cost. The following analysis quantitatively determines when this design strategy has likely volume, mass, or cost benefit.

Recall from (3), the stored energy in a particular (linear) capacitor at an applied voltage V_a is expressed as

$$E_\mathrm{a} = \frac{1}{2} C V_\mathrm{a}^2 \tag{23}$$

thus the consequent applied volumetric energy density $\gamma_\mathrm{v,a}$ of the *underutilized* capacitor is

$$\gamma_\mathrm{v,a}(V_\mathrm{a}) = \frac{E_\mathrm{a}}{\mathrm{Vol}} = \frac{\gamma_\mathrm{v}}{V_\mathrm{r}^2} V_\mathrm{a}^2. \tag{24}$$

This derated energy density $\gamma_\mathrm{v,a}$ scales quadratically with the applied voltage V_a justifying its +40 dB/decade slope indicated by the dashed lines in Fig. 12a.

Besides enabling juxtaposition of individual capacitors, the empirical data also indicates the peak performance capability of the whole technology.

The 'best' capacitor has the best FOM and lies on the Pareto front of the comprehensively surveyed data set. Figure 12a illustrates the empirically derived Pareto fronts $f_\mathrm{P}(V_\mathrm{r})$ for volumetric energy density γ_v as a function of rated voltage V_r for major capacitor technologies: aluminum electrolytic, tantalum electrolytic, Class I ceramic, Class II ceramic, and film. For each capacitor data set, the derivative of its Pareto curve $f'_\mathrm{P}(V_\mathrm{r})$ can exceed $\gamma'_\mathrm{v,a}(V_\mathrm{a})$, the derivative of the derated energy density curve in (24), below a specific critical rated voltage $V_\mathrm{r,crit}$:

$$f'_\mathrm{P}(V_\mathrm{r}) > \gamma'_\mathrm{v,a}(V_\mathrm{a}) = \frac{\mathrm{d}}{\mathrm{d}V_\mathrm{a}} \left(\frac{\gamma_\mathrm{v}}{V_\mathrm{r}^2} V_\mathrm{a}^2 \right) = \frac{2\gamma_\mathrm{v}}{V_\mathrm{r}^2} V_\mathrm{a}. \tag{25}$$

Evaluating this inequality for components on the Pareto curve ($\gamma_\mathrm{v} = f_\mathrm{P}(V_\mathrm{r})$) and at a rated voltage application ($V_\mathrm{a} = V_\mathrm{r}$) yields

$$f_\mathrm{P}(V_\mathrm{r,crit}) = \frac{1}{2} V_\mathrm{r,crit}\, f'_\mathrm{P}(V_\mathrm{r,crit}). \tag{26}$$

The critical rated voltage $V_\mathrm{r,crit}$ is the rated voltage satisfying this equality comprised of the Pareto curve and its gradient.

In Figure 12a, every capacitor (not just Pareto optimal components) with voltage rating less than the critical inflection point $V_\mathrm{r} < V_\mathrm{r,crit}$ has a larger volume than the highest volumetric energy density γ_v capacitor with rated voltage $V_\mathrm{r} = V_\mathrm{r,crit}$ when derated to any applied voltage. In summary to minimize volume, an overrated capacitor with $V_\mathrm{r} = V_\mathrm{r,crit}$ should always be sought when $V_\mathrm{a} < V_\mathrm{r,crit}$. For capacitors with rated voltages above this critical inflection point $V_\mathrm{r} > V_\mathrm{r,crit}$, it is preferable to avoid voltage derating beyond that which is practically necessary; the volume-minimized capacitor has a voltage rating nearer to the applied voltage or $V_\mathrm{r} = V_\mathrm{a}$.

A similar process yields the critical rated voltage for the gravimetric (or specific) energy density $\gamma_\mathrm{m} = \frac{E_\mathrm{r}}{\mathrm{Mass}}$ and the energy per cost $\gamma_\mathrm{c} = \frac{E_\mathrm{r}}{\mathrm{Cost}}$ as shown in Fig. 12b and Fig. 12c, respectively. All critical rated voltages $V_\mathrm{r,crit}$ for energy density γ with respect to volume, mass, and cost are tabulated in Table IV. Inspection of Fig. 12 reveals aluminum electrolytic capacitors notably do not have a critical rated voltage with respect to volume or mass, thus efficient component selection should nearly always adhere to $V_\mathrm{r} = V_\mathrm{a}$ for this capacitor technology. Interestingly, Fig. 12c reveals that film capacitors with $V_\mathrm{r} < 300\,\mathrm{V}$ should not be selected to minimize cost since the best $V_\mathrm{r} = 300\,\mathrm{V}$ device proves to be more cost effective, even when derated to lower voltages.

Finally, practical margins of rated voltages (per each capacitor technology) can be incorporated into the analysis of the data. This includes innate self-healing and over-voltage properties in film and ceramic capacitor technologies, as well as conventional voltage derating such as for tantalum electrolytic capacitors [52].

B. Capacitor Energy Density

The comprehensive data allows consideration of energy density trends in particular capacitor technologies. For instance, as mentioned in [48], the achievable volumetric and gravimetric energy density γ_v and γ_m of aluminum electrolytic capacitors approximately increases linearly with rated voltage V_r; this trend is confirmed by the Pareto fronts (for $V_\mathrm{r} < 450\,\mathrm{V}$) in Fig. 12.

The acquired data also allows comparison in the energy storage capabilities of different capacitor technologies. The Pareto curves in Fig. 12 indicate certain capacitor technologies dominate at various rated voltages with respect to volume,

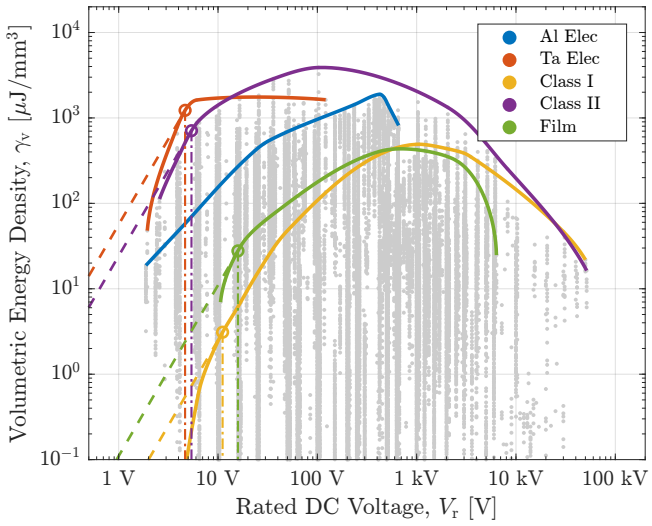

(a) Rated dc voltage V_r versus volumetric energy density γ_v

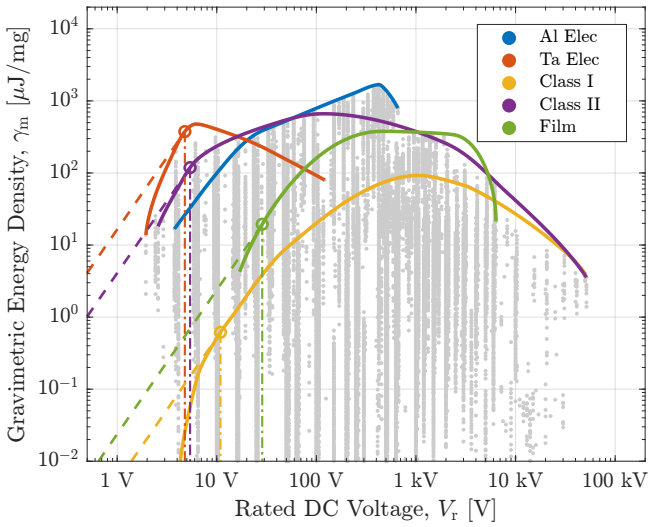

(b) Rated dc voltage V_r versus gravimetric energy density γ_m

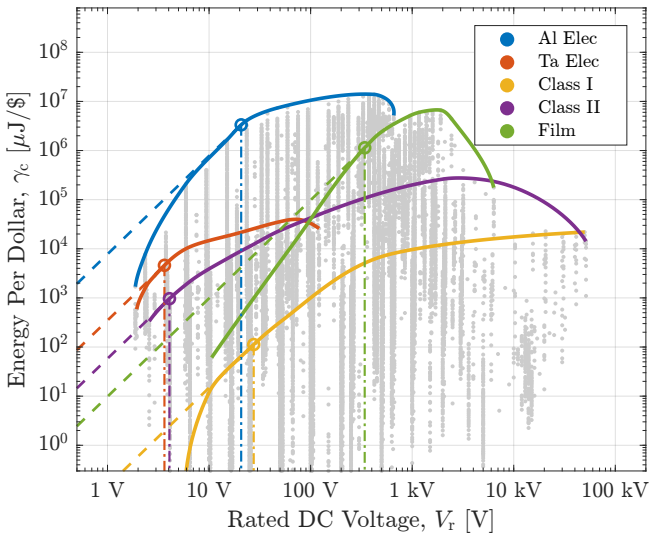

(c) Rated dc voltage V_r versus energy per cost γ_c

Fig. 12. Commercial capacitor energy density FOM—(a) volume, (b) mass, and (c) cost—of the comprehensive data set across common technologies. The Pareto fronts are highlighted as well as the critical rated voltage $V_{r,crit}$ where capacitor voltage overrating becomes useful.

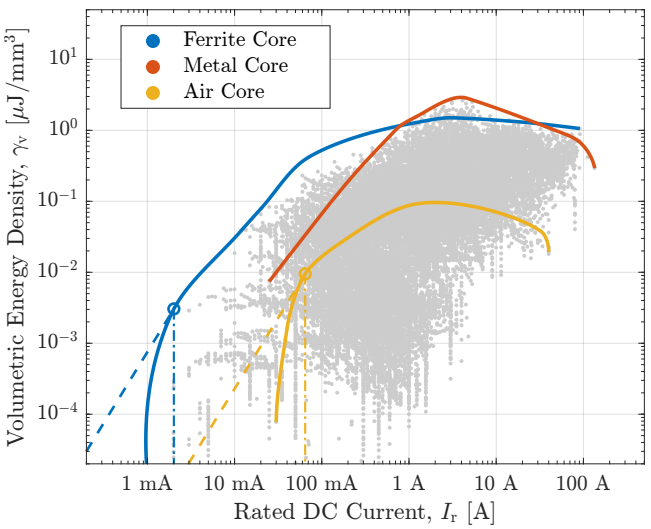

(a) Rated dc current I_r versus volumetric energy density γ_v

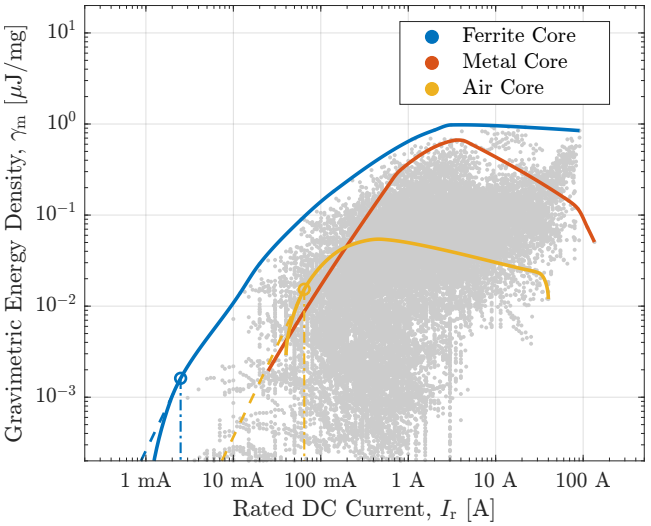

(b) Rated dc current I_r versus gravimetric energy density γ_m

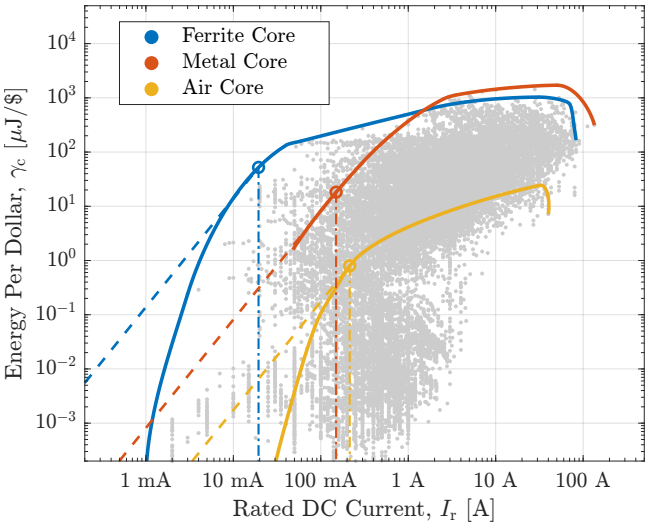

(c) Rated dc current I_r versus energy per cost γ_c

Fig. 13. Commercial inductor energy density FOM—(a) volume, (b) mass, and (c) cost—of the comprehensive data set across common technologies. The Pareto fronts are highlighted as well as the critical rated current $I_{r,crit}$ where inductor current overrating becomes useful.

TABLE IV
SUMMARY OF CRITICAL VOLTAGES FOR CAPACITOR OVERRATING

	Al Elec	Ta Elec	Class I	Class II	Film
Volume	N/A	5 V	10 V	5 V	11 V
Mass	N/A	5 V	10 V	5 V	12 V
Cost	12 V	4 V	12 V	4 V	300 V

TABLE V
SUMMARY OF CRITICAL CURRENTS FOR INDUCTOR OVERRATING

	Ferrite	Metal	Air
Volume	2.0 mA	N/A	60 mA
Mass	2.5 mA	N/A	65 mA
Cost	20 mA	150 mA	200 mA

mass, and cost. For $V_\mathrm{r} < 10\,\mathrm{V}$, tantalum electrolytic capacitors have the largest energy densities and thus the smallest volume and mass. In the $10\,\mathrm{V} < V_\mathrm{r} < 700\,\mathrm{V}$ range, aluminum electrolytic capacitors are the lightest and Class II ceramic capacitors are the smallest. Above $V_\mathrm{r} > 1\,\mathrm{kV}$, both Class II ceramic and film capacitors are superior with respect to mass, while only Class II ceramic capacitors are superior with respect to volume. Aluminum electrolytic capacitors are the lowest cost solution to fulfill system energy requirements for $V_\mathrm{r} < 700\,\mathrm{V}$ as claimed in [41], [48], whereas film capacitors are the lowest cost for $700\,\mathrm{V} < V_\mathrm{r} < 6\,\mathrm{kV}$, and ceramics are the lowest cost for $V_\mathrm{r} > 6\,\mathrm{kV}$. Class I ceramic capacitors are ubiquitously poor performers with respect to energy density except at the highest rated voltages $V_\mathrm{r} > 10\,\mathrm{kV}$.

C. Inductor Current Overrating

The comprehensive data set can also produce the conditions for useful inductor current overrating. By following an analogous derivation as Section VI-A, the critical rated current $I_\mathrm{r,crit}$ is derived for ferrite, metal, and air core inductor technologies since the energy stored in a linear inductor at an applied dc current I_a is

$$E_\mathrm{a} = \frac{1}{2} L I_\mathrm{a}^2. \tag{27}$$

Fig. 13 illustrates the technological subsets and their Pareto fronts for rated current I_r versus volumetric energy density γ_v, gravimetric energy density γ_m, and energy per cost γ_c, respectively. Table V tabulates the resulting critical current ratings $I_\mathrm{r,crit}$ for each technology, i.e., the lower limit below which no advantage is gained for devices with a reduced current rating.

D. Inductor Energy Density

The comprehensive data reveals the energy storage capabilities of inductors with respect to core material. Ferrite cores are the most energy-dense core type with respect to mass. With respect to volume and cost, ferrite core inductors are the most energy-dense for rated current $I_\mathrm{r} < 1\,\mathrm{A}$, while above $I_\mathrm{r} > 1\,\mathrm{A}$, both ferrite and metal core technologies dominate. The best air core inductors have a consistent 10–100$\times$ lower energy density (with respect to volume, mass, and cost) than the best-performing ferrite and metal core inductors, although they compete equally with metal core inductors with respect to mass for current ratings below $I_\mathrm{r} < 200\,\mathrm{mA}$.

E. Comparing Capacitors and Inductors

Modern power converter topologies increasingly leverage the performance of capacitors versus inductors: hybrid switched-capacitor converters such as the FCML converter [11], [97], [104], series-capacitor buck converter [16]–[18], and switching bus converter [105], [106]. The fundamental trade-off between these energy storage elements requires the careful quantification of realizable device performance.

Some passive component FOM are jointly applicable to both capacitors and inductors—two fundamentally different circuit elements—and once these FOM are identified, these components can be justly compared. Energy density γ is one such generic FOM, as rated energy storage is well defined for both capacitors in (18) and inductors in (19). From the comprehensive data set, Fig. 14 conveys that there is a marked difference in the energy density capabilities of commercial capacitors and inductors. As a whole, the highest volumetric energy density γ_v commercial capacitor devices are nearly 1,000$\times$ greater than that of the highest γ_v commercial inductors. For volume-sensitive applications, choosing a circuit topology that heavily utilizes capacitors as energy transfer elements can result in a more volume efficient design [11], [13], [104], [107], [108].

Similarly for gravimetric energy density γ_m and energy per cost γ_c, the best commercial capacitors outperform the best commercial inductors by a factor of nearly 2,000 and 10,000, respectively. Thus, capacitor-dominant circuit topologies are even more heavily favored for cost and mass-optimized designs than for volume-optimized designs.

It should be noted that, unlike capacitors, custom inductors are capable of achieving markedly higher performance than their commercial counterparts [1], [70], [71], [109]. Further work may subsequently explore the capabilities of custom inductor constructions, with the benchmarks for commercial inductors firmly established in this work as reference.

F. Future Applications

Now armed with precisely quantitative intuition for inductor and capacitor performance, various device FOM can be further incorporated into analytical and procedural design methodologies for power electronics design. This work compliments recently developed analyses allowing for the design of optimized hybrid switched-capacitor converters [15], [107], [108], [110]. Work in [64] analytically links capacitor energy density FOM and power density FOM to the operating waveforms of an aluminum electrolytic dc-link capacitor bank designed for single-phase twice-line frequency power buffering. Both

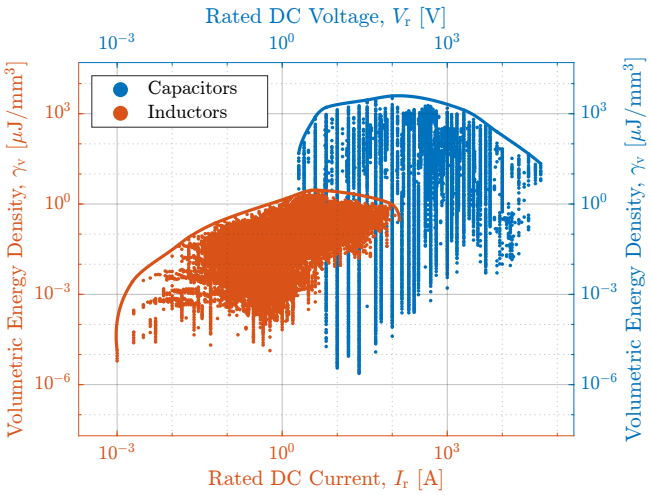

(a) Rated dc voltage V_r / current I_r versus volumetric energy density γ_v

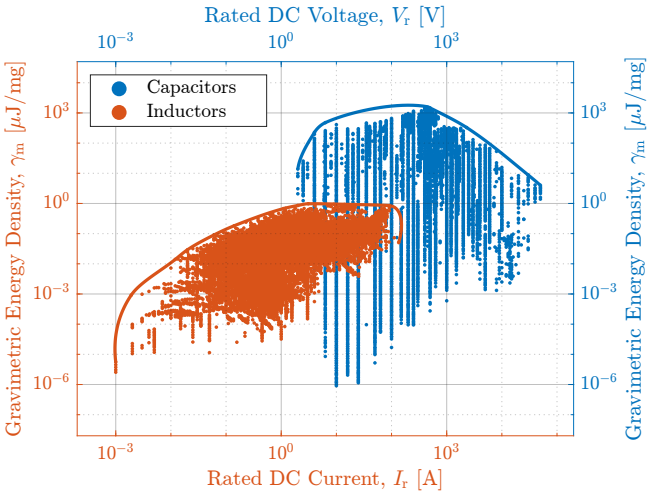

(b) Rated dc voltage V_r / current I_r versus gravimetric energy density γ_m

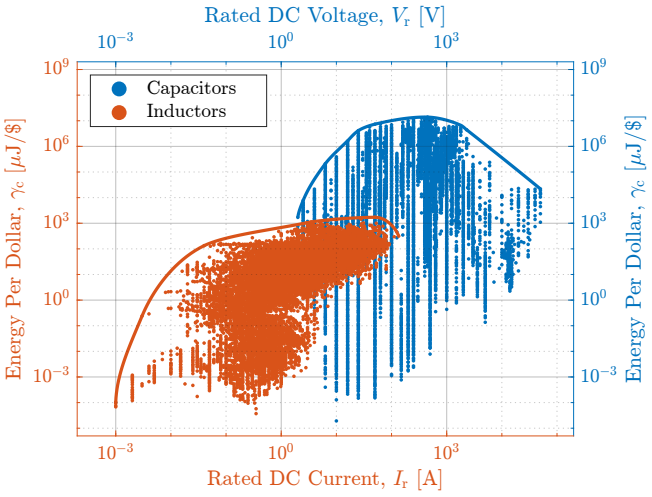

(c) Rated dc voltage V_r / current I_r versus energy per cost γ_c

Fig. 14. Commercial capacitor versus inductor energy density FOM—(a) volume, (b) mass, and (c) cost—of the comprehensive data set. From the highlighted Pareto fronts, commercial capacitors have a roughly $1,000\times$ better maximum energy density capability compared to commercial inductors with respect to volume, a roughly $2,000\times$ improvement with respect to mass, and a roughly $10,000\times$ improvement with respect to cost.

of these applications, and many others, require actual device FOM for optimal design and demonstrate the utility of the data presented in this work.

Finally, the comprehensive data set can continue to be improved as manufacturers and distributors standardize and digitally disseminate more passive component information.

VII. Conclusion

The true technological capabilities of electrical devices are historically difficult to quantify due to the immense variety of components currently in development, commercially available to consumers, or entirely obsolete. Utilizing modern advancements in the accessibility of public, large-scale, and digitized component data, a phenomenological framework is developed yielding definitive and quantified component performance. This work reviews methods of broad passive component characterization and it presents a methodology for developing robust device figures-of-merit (FOM) to benchmark and compare passive—capacitor and inductor—components. This framework is directly applied to the data for 606,000 commercial capacitors and 88,000 commercial inductors.

Sampled data collection and measurement are used to supplement deficiencies in the comprehensive data set. To generate information on energy storage, this work presents an empirical fit for estimating the energy-equivalent capacitance of Class II (and Class III) ceramic capacitors. The fit was validated on 2550 datasheet characteristic capacitance (or C-V) curves and produces a mean error of 3.1% for energy-equivalent capacitance at rated voltage $C_E(V_r)$. This work also presents empirical constant and power expression fits in Table III for estimating the volumetric mass density $D = \frac{\text{Mass}}{\text{Vol}}$ of a passive component from its rated voltage and capacitance for capacitors in (21), and rated current and inductance for inductors in (22). The empirical fits are generated from 447 device volume and mass measurements across various capacitor and inductor technologies, and produce a worst-case mean percentage error of 20%.

This work then specifically investigates trends in capacitor and inductor stored energy density with respect to volume, mass, and cost. Analysis of the entire data set for each component technology reveals the minimum useful capacitor rated voltage for the purposes of voltage overrating; similar critical rated currents are derived for inductor technologies. Recommendations for minimum useful component overvoltage/overcurrent ratings are tabulated in Table IV and Table V.

This work aims to justify particular device FOM and provides an explicit reference for practicing engineers when selecting passive components and designing circuits.

VIII. Acknowledgements

The information, data aggregation, and work presented herein were funded in part by the National Science Foundation Graduate Research Fellowship Program under Grant No. 2146752; the Advanced Research Projects Agency-Energy (ARPA-E), U.S. Department of Energy, under Award Number DE-AR0000900; and Enphase Energy. Any opinions, findings, and conclusions or recommendations expressed in this material

are those of the author(s) and do not necessarily reflect the views of these organizations.

The authors acknowledge Dr. Bradley Bowles for his insights into linear regression and meaningful statistical measures, Shalin Shah for his tangential yet influential work rigorously collecting and visualizing massive component data sets, and both Professor Jessica Boles and Elisa Krause for their editorial reviews. The authors also acknowledge Digikey Electronics; TDK Corporation; and Octopart, Inc. for conglomerating the digitized component data which forms the foundation of this work.

REFERENCES

[1] C. R. Sullivan, B. A. Reese, A. L. F. Stein, and P. A. Kyaw, "On size and magnetics: Why small efficient power inductors are rare," in *2016 International Symposium on 3D Power Electronics Integration and Manufacturing (3D-PEIM)*, Jun. 2016, pp. 1–23.

[2] S. Qin, Y. Lei, C. Barth, W.-C. Liu, and R. C. N. Pilawa-Podgurski, "A high-efficiency high energy density buffer architecture for power pulsation decoupling in grid-interfaced converters," in *2015 IEEE Energy Conversion Congress and Exposition (ECCE)*, Sep. 2015, pp. 149–157.

[3] S. Coday and R. C. N. Pilawa-Podgurski, "Characterization and modeling of ceramic capacitor losses under large signal operating conditions," *IEEE Open J. Power Electron.*, vol. 4, pp. 24–33, 2023.

[4] J. Zou, N. C. Brooks, S. Coday, N. M. Ellis, and R. C. Pilawa-Podgurski, "On the size and weight of passive components: Scaling trends for high-density power converter designs," in *2022 IEEE 23rd Workshop on Control and Modeling for Power Electronics (COMPEL)*, Jun. 2022, pp. 1–7.

[5] J. Rodriguez, J.-S. Lai, and F. Z. Peng, "Multilevel inverters: A survey of topologies, controls, and applications," *IEEE Trans. Ind. Electron.*, vol. 49, pp. 724–738, Aug. 2002.

[6] E. Solas, G. Abad, J. A. Barrena, S. Aurtenetxea, A. Cárcar, and L. Zajac, "Modular multilevel converter with different submodule concepts—Part I: Capacitor voltage balancing method," *IEEE Trans. Ind. Electron.*, vol. 60, pp. 4525–4535, Jul. 2013.

[7] M. A. Perez, S. Bernet, J. Rodriguez, S. Kouro, and R. Lizana, "Circuit topologies, modeling, control schemes, and applications of modular multilevel converters," *IEEE Trans. Power Electron.*, vol. 30, pp. 4–17, Jan. 2015.

[8] A. Dekka, B. Wu, R. L. Fuentes, M. Perez, and N. R. Zargari, "Evolution of topologies, modeling, control schemes, and applications of modular multilevel converters," *IEEE Trans. Emerg. Sel. Topics Power Electron.*, vol. 5, pp. 1631–1656, Dec. 2017.

[9] T. Meynard and H. Foch, "Multi-level conversion: high voltage choppers and voltage-source inverters," in *PESC '92 Record. 23rd Annual IEEE Power Electronics Specialists Conference*, vol. 1, Aug. 1992, pp. 397–403.

[10] B. P. McGrath and D. G. Holmes, "Natural capacitor voltage balancing for a flying capacitor converter induction motor drive," *IEEE Trans. Power Electron.*, vol. 24, pp. 1554–1561, Jun. 2009.

[11] Y. Lei *et al.*, "A 2-kw single-phase seven-level flying capacitor multilevel inverter with an active energy buffer," *IEEE Trans. Power Electron.*, vol. 32, pp. 8570–8581, Nov. 2017.

[12] B. Axelrod, Y. Berkovich, and A. Ioinovici, "Switched-capacitor/switched-inductor structures for getting transformerless hybrid dc-dc pwm converters," *IEEE Trans. Circuits Syst. I*, vol. 55, pp. 687–696, Mar. 2008.

[13] Y. Lei, W.-C. Liu, and R. C. N. Pilawa-Podgurski, "An analytical method to evaluate and design hybrid switched-capacitor and multilevel converters," *IEEE Trans. Power Electron.*, vol. 33, pp. 2227–2240, Mar. 2018.

[14] C. Schaef, J. Rentmeister, and J. T. Stauth, "Multimode operation of resonant and hybrid switched-capacitor topologies," *IEEE Trans. Power Electron.*, vol. 33, pp. 10 512–10 523, Dec. 2018.

[15] P. H. McLaughlin, J. S. Rentmeister, M. H. Kiani, and J. T. Stauth, "Analysis and comparison of hybrid-resonant switched-capacitor dc-dc converters with passive component size constraints," *IEEE Trans. Power Electron.*, vol. 36, pp. 3111–3125, Mar. 2021.

[16] K. Nishijima, K. Harada, T. Nakano, T. Nabeshima, and T. Sato, "Analysis of double step-down two-phase buck converter for VRM," in *INTELEC 05 - Twenty-Seventh International Telecommunications Conference*, Mar. 2005, pp. 497–502.

[17] Y. Jang, M. Jovanovic, and Y. Panov, "Multiphase buck converters with extended duty cycle," in *Twenty-First Annual IEEE Applied Power Electronics Conference and Exposition, 2006. APEC '06.*, Mar. 2006, pp. 38–44.

[18] P. S. Shenoy, M. Amaro, J. Morroni, and D. Freeman, "Comparison of a buck converter and a series capacitor buck converter for high-frequency, high-conversion-ratio voltage regulators," *IEEE Trans. Power Electron.*, vol. 31, pp. 7006–7015, Oct. 2016.

[19] R. Steigerwald, "A comparison of half-bridge resonant converter topologies," *IEEE Trans. Power Electron.*, vol. 3, pp. 174–182, Apr. 1988.

[20] K. Jin, X. Ruan, M. Yang, and M. Xu, "A hybrid fuel cell power system," *IEEE Trans. Ind. Electron.*, vol. 56, pp. 1212–1222, Apr. 2009.

[21] X. Li and A. K. S. Bhat, "Analysis and design of high-frequency isolated dual-bridge series resonant dc/dc converter," *IEEE Trans. Power Electron.*, vol. 25, pp. 850–862, Apr. 2010.

[22] B. Lu, W. Liu, Y. Liang, F. Lee, and J. van Wyk, "Optimal design methodology for LLC resonant converter," in *Twenty-First Annual IEEE Applied Power Electronics Conference and Exposition, 2006. APEC '06.*, Mar. 2006, pp. 533–538.

[23] J. Deng, S. Li, S. Hu, C. C. Mi, and R. Ma, "Design methodology of LLC resonant converters for electric vehicle battery chargers," *IEEE Trans. Veh. Technol.*, vol. 63, pp. 1581–1592, May 2014.

[24] D. Menzi, M. Heller, and J. W. Kolar, "iGSE-C_x - A new normalized Steinmetz model for Class II multilayer ceramic capacitors," *IEEE Open J. Power Electron.*, vol. 2, pp. 138–144, Feb. 2021.

[25] D. Menzi *et al.*, "iGSE-CD—An electric-/displacement-field related Steinmetz model for Class II multilayer ceramic capacitors under low-frequency large-signal excitation," *IEEE Open J. Power Electron.*, vol. 4, pp. 107–116, Jan. 2023.

[26] Y. Jiang *et al.*, "Loss characterization and modeling of class ii multilayer ceramic capacitors: A synergic material-microstructure-device approach," *IEEE Trans. Power Electron.*, pp. 1–20, 2023.

[27] M. Solomentsev and A. J. Hanson, "At what frequencies should air-core magnetics be used?" *IEEE Trans. Power Electron.*, vol. 38, pp. 3546–3558, Mar. 2023.

[28] J. Azurza Anderson, G. Zulauf, J. W. Kolar, and G. Deboy, "New figure-of-merit combining semiconductor and multi-level converter properties," *IEEE Open J. Power Electron.*, vol. 1, pp. 322–338, Aug. 2020.

[29] C. B. Barth, T. Foulkes, I. Moon, Y. Lei, S. Qin, and R. C. N. Pilawa-Podgurski, "Experimental evaluation of capacitors for power buffering in single-phase power converters," *IEEE Trans. Power Electron.*, vol. 34, pp. 7887–7899, Oct. 2019.

[30] B. R. Hayworth, "The behavior of polyester film energy storage capacitors," *IEEE Trans. Electr. Insul.*, vol. EI-3, pp. 47–49, May 1968.

[31] T. Ashburn and D. J. Skamser, "Highly accelerated testing of capacitors for medical applications," in *Proceedings of the 5th SMTA Medical Electronics Symposium*, Jan. 2008.

[32] L. Mei, "Highly accelerated life stress testing (halst) of base-metal electrode multilayer ceramic capacitors," in *Proceedings of CARTS International: The 33rd Symposium for Passive Electronic Components*, 2013, pp. 217–234.

[33] A. J. Hanson, J. A. Belk, S. Lim, C. R. Sullivan, and D. J. Perreault, "Measurements and performance factor comparisons of magnetic materials at high frequency," *IEEE Trans. Power Electron.*, vol. 31, pp. 7909–7925, Nov. 2016.

[34] T. Foulkes, T. Modeer, and R. C. N. Pilawa-Podgurski, "Quantifying dynamic on-state resistance of GaN HEMTs for power converter design via a survey of low and high voltage devices," *IEEE Trans. Emerg. Sel. Topics Power Electron.*, vol. 9, pp. 4036–4049, Aug. 2021.

[35] H. Li, S. R. Lee, M. Luo, C. R. Sullivan, Y. Chen, and M. Chen, "Magnet: A machine learning framework for magnetic core loss modeling," in *2020 IEEE 21st Workshop on Control and Modeling for Power Electronics (COMPEL)*, Nov. 2020, pp. 1–8.

[36] H. Li *et al.*, "Magnet: An open-source database for data-driven magnetic core loss modeling," in *2022 IEEE Applied Power Electronics Conference and Exposition (APEC)*, Mar. 2022, pp. 588–595.

[37] S. Reese and D. Maksimovic, "An approach to dc-dc converter optimization using machine learning-based component models," in *2022 IEEE 23rd Workshop on Control and Modeling for Power Electronics (COMPEL)*, Jun. 2022, pp. 1–8.

[38] T. R. Burkes, M. Hagler, M. Kristiansen, J. Craig, W. Portnoy, and E. Kunhardt, "A critical analysis and assessment of high power switches," Southeastern Center for Electrical Engineering Education Inc., St. Cloud, FL, Tech. Rep., 1978.

[39] S. Reese *et al.*, "Loss estimation and design of dc-dc converters using physics- and data-based component models," in *2023 IEEE Applied Power Electronics Conference and Exposition (APEC)*, Jun. 2023, pp. 82–89.

[40] J. W. Kolar, J. Biela, S. Waffler, T. Friedli, and U. Badstuebner, "Performance trends and limitations of power electronic systems," in *2010 6th International Conference on Integrated Power Electronics Systems*, Mar. 2010, pp. 1–20.

[41] J. Both, "Electrolytic capacitors from the postwar period to the present," *IEEE Electr. Insul. Mag.*, vol. 32, pp. 8–26, Mar. 2016.

[42] S. Havanur, "Rethinking the power MOSFET figure of merit," *Technical Articles*, Mar. 2017. [Online]. Available: https://eepower.com/technical-articles/rethinking-the-power-mosfet-figure-of-merit/#

[43] M. Randall *et al.*, "The battle for maximum volumetric efficiency—Part 2: Advancements in solid electrolyte capacitors," in *CARTS Europe 2007*, Nov. 2007, pp. 11–22.

[44] A. Lidow, D. Kinzer, G. Sheridan, and D. Tam, "The semiconductor roadmap for power management in the new millennium," *Proc. IEEE*, vol. 89, pp. 803–812, Jun. 2001.

[45] M. Kasper, D. Bortis, and J. W. Kolar, "Scaling and balancing of multi-cell converters," in *2014 International Power Electronics Conference (IPEC-Hiroshima 2014 - ECCE ASIA)*, May 2014, pp. 2079–2086.

[46] M. A. Green, "Third generation photovoltaics: Ultra-high conversion efficiency at low cost," *Progress in Photovoltaics: Research and Applications*, vol. 9, pp. 123–135, Apr. 2001. [Online]. Available: https://onlinelibrary.wiley.com/doi/abs/10.1002/pip.360

[47] A. Bidram, A. Davoudi, and R. S. Balog, "Control and circuit techniques to mitigate partial shading effects in photovoltaic arrays," *IEEE J. Photovolt.*, vol. 2, pp. 532–546, Oct. 2012.

[48] W. Sarjeant, "Capacitor fundamentals," in *Proceedings of the 19th Electrical Electronics Insulation Conference,*, Sep. 1989, pp. 1–51.

[49] Y. Wang, X. Zhou, Q. Chen, B. Chu, and Q. Zhang, "Recent development of high energy density polymers for dielectric capacitors," *IEEE Trans. Dielectr. Electr. Insul.*, vol. 17, pp. 1036–1042, Aug. 2010.

[50] Y. Li *et al.*, "Multilayered ferroelectric polymer composites with high energy density at elevated temperature," *Composites Science and Technology*, vol. 202, Dec. 2021. [Online]. Available: https://www.sciencedirect.com/science/article/pii/S026635382032385X

[51] J. Ennis, Y. H. Yang, F. MacDougall, K. Seal, and J. Herbig, "High energy density capacitor characterization," in *Conference Record of the Twenty-Sixth International Power Modulator Symposium, 2004 and 2004 High-Voltage Workshop.*, 2004, pp. 68–71.

[52] R. Hahn, M. Randall, and J. Paulsen, "The battle for maximum volumetric efficiency—Part 1: When technologies compete, customers win," in *CARTS Europe 2007*, Nov. 2007, pp. 47–57.

[53] S. Kwon, W. Hackenberger, E. Alberta, E. Furman, and M. Lanagan, "Nonlinear dielectric ceramics and their applications to capacitors and tunable dielectrics," *IEEE Electr. Insul. Mag.*, vol. 27, pp. 43–55, Mar. 2011.

[54] A. Chauhan, S. Patel, R. Vaish, and C. R. Bowen, "Anti-ferroelectric ceramics for high energy density capacitors," *Materials*, vol. 8, pp. 8009–8031, Nov. 2015. [Online]. Available: https://www.mdpi.com/1996-1944/8/12/5439

[55] S. Cheema *et al.*, "Giant energy storage ultrafast microsupercapacitors via negative capacitance superlattices," submitted for publication. [Online]. Available: https://www.researchsquare.com/article/rs-2420676/v1

[56] J. R. MacDonald, M. A. Schneider, J. B. Ennis, F. W. MacDougall, and X. H. Yang, "High energy density capacitors," in *2009 IEEE Electrical Insulation Conference*, May 2009, pp. 306–309.

[57] *Pulse Discharge, High Voltage, High Temperature 200 °C C0G Dielectric, 1,000 VDC – 3,500 VDC (Industrial Grade)*, KEMET Corporation, Dec. 2022. [Online]. Available: https://content.kemet.com/datasheets/KEM_C1035_C0G_PULSE_SMD.pdf

[58] T. R. Jow *et al.*, "Pulsed power capacitor development and outlook," in *2015 IEEE Pulsed Power Conference (PPC)*, May 2015, pp. 1–7.

[59] N. Kularatna and K. Gunawardane, *Energy Storage Devices for Renewable Energy-Based Systems*, 2nd ed. Boston: Academic Press, 2021, ch. 2, pp. 37–64. [Online]. Available: https://www.sciencedirect.com/science/article/pii/B978012820778900005X

[60] S. Chowdhury, E. Gurpinar, and B. Ozpineci, "Capacitor technologies: Characterization, selection, and packaging for next-generation power electronics applications," *IEEE Trans. Transport. Electrific.*, vol. 8, pp. 2710–2720, Jun. 2022.

[61] W. Sarjeant, I. Clelland, and R. Price, "Capacitive components for power electronics," *Proc. IEEE*, vol. 89, pp. 846–855, Jun. 2001.

[62] J. Connolly and M. Dunn, "High energy density capacitor development at ABB power T&D," in *ICSD'98. Proceedings of the 1998 IEEE 6th International Conference on Conduction and Breakdown in Solid Dielectrics (Cat. No.98CH36132)*, Jun. 1998, pp. 110–113.

[63] T. Scholz, P. Winsor, and M. Hudis, "Development of a high energy density storage capacitor for NIF," in *Digest of Technical Papers. 12th IEEE International Pulsed Power Conference. (Cat. No.99CH36358)*, vol. 1, Jun. 1999, pp. 114–117.

[64] N. C. Brooks, F. Giardine, and R. C. Pilawa-Podgurski, "Dc-link capacitors for twice-line frequency power decoupling: Design-oriented figures-of-merit with empirical application," *IEEE Power Electron. Lett.*, submitted for publication.

[65] H. Wang and F. Blaabjerg, "Reliability of capacitors for dc-link applications in power electronic converters - an overview," *IEEE Trans. Ind. Appl.*, vol. 50, pp. 3569–3578, Sep. 2014.

[66] Y. Han, G. Cheung, A. Li, C. R. Sullivan, and D. J. Perreault, "Evaluation of magnetic materials for very high frequency power applications," *IEEE Trans. Power Electron.*, vol. 27, pp. 425–435, Jan. 2012.

[67] *IEEE Standard for Test Procedures for Magnetic Cores*, Std. 393-1991, 1992.

[68] K. Kabeya, S. Yanase, Y. Okazaki, and K. Yun, "Magnetic property of iron-dust cores with mixture of ferromagnetic ferrite powder and alumina powder," *IEEE Trans. Magn.*, vol. 50, pp. 1–4, Apr. 2014.

[69] H. Lin *et al.*, "Voltage tunable magnetoelectric inductors with improved operational frequency and quality factor for power electronics," *IEEE Trans. Magn.*, vol. 51, pp. 1–5, Jan. 2015.

[70] R. S. Yang, A. J. Hanson, B. A. Reese, C. R. Sullivan, and D. J. Perreault, "A low-loss inductor structure and design guidelines for high-frequency applications," *IEEE Trans. Power Electron.*, vol. 34, pp. 9993–10 005, Oct. 2019.

[71] R. S. Bayliss, R. S. Yang, A. J. Hanson, C. R. Sullivan, and D. J. Perreault, "Design, implementation, and evaluation of high-efficiency high-power radio-frequency inductors," in *2021 IEEE Applied Power Electronics Conference and Exposition (APEC)*, Mar. 2021, pp. 881–888.

[72] *Ferrites and accessories*, TDK Corporation, Feb. 2023. [Online]. Available: https://www.tdk-electronics.tdk.com/download/528870/80183d6ef4a48b49c5bee48a6e8b2ac5/pdf-n48.pdf

[73] W. A. Roshen, "A practical, accurate and very general core loss model for nonsinusoidal waveforms," *IEEE Trans. Power Electron.*, vol. 22, pp. 30–40, Jan. 2007.

[74] D. Cittanti *et al.*, "Analysis, design and experimental assessment of a high power density ceramic dc-link capacitor for a 800 V 550 kVA electric vehicle drive inverter," *IEEE Trans. Ind. Appl.*, submitted for publication.

[75] M.-J. Pan and C. A. Randall, "A brief introduction to ceramic capacitors," *IEEE Electr. Insul. Mag.*, vol. 26, pp. 44–50, May/Jun. 2010.

[76] D. Neumayr, G. C. Knabben, E. Varescon, D. Bortis, and J. W. Kolar, "Comparative evaluation of a full- and partial-power processing active power buffer for ultracompact single-phase dc/ac converter systems," *IEEE Trans. Emerg. Sel. Topics Power Electron.*, vol. 9, pp. 1994–2013, Apr. 2021.

[77] K. Kubota and S. Nishiyama, "Ceramic capacitors aid high-voltage designs," May 2004. [Online]. Available: https://www.electronicdesign.com/content/article/21187205/ceramic-capacitors-aid-highvoltage-designs

[78] *General Descriptions of Aluminum Electrolytic Capacitors*, Nichicon Corporation. [Online]. Available: https://www.nichicon.co.jp/english/products/pdf/aluminum.pdf

[79] *Aluminum Electrolytic Capacitor Application Guide*, Cornell Dubilier Electronics, 2023. [Online]. Available: https://www.cde.com/resources/technical-papers/AEappGuide.pdf

[80] C. P. Steinmetz, "On the law of hysteresis," *IEEE Trans. Amer. Inst. of Elect. Engineers*, vol. IX, pp. 1–64, Jan. 1892.

[81] K. Venkatachalam, C. Sullivan, T. Abdallah, and H. Tacca, "Accurate prediction of ferrite core loss with nonsinusoidal waveforms using only Steinmetz parameters," in *2002 IEEE Workshop on Computers in Power Electronics, 2002. Proceedings.*, Jun. 2002, pp. 36–41.

[82] W. Sarjeant, J. Zirnheld, and F. MacDougall, "Capacitors," *IEEE Trans. Plasma Sci.*, vol. 26, pp. 1368–1392, Oct. 1998.

[83] N. C. Brooks and R. C. N. Pilawa-Podgurski, "Hybrid switched-capacitor converter design: State-space dynamical modeling and passive device characterization," Ph.D. dissertation, EECS Department,

University of California, Berkeley, Aug 2023. [Online]. Available: http://www2.eecs.berkeley.edu/Pubs/TechRpts/2023/EECS-2023-218.html

[84] *Ceramic Dielectric Capacitors, Classes I, II, III, and IV, Part II: Test Methods*, Electronics Components Industry Association Std. EIA-198-2, Rev. E, Jan. 1998.

[85] *Fixed capacitors for use in electronic equipment - Part 1: Generic specification*, International Electrotechnical Commission Std. IEC-60384-1:2021, Rev. 6.0, Feb. 2021.

[86] *General Specification for Capacitor, Fixed, Ceramic Dielectric (General Purpose)*, Naval Publications and Form Center Std. MIL-C-11015, Rev. G, Jul. 2017.

[87] D. Costinett, D. Maksimovic, and R. Zane, "Circuit-oriented treatment of nonlinear capacitances in switched-mode power supplies," *IEEE Trans. Power Electron.*, vol. 30, pp. 985–995, Mar. 2015.

[88] M. Kasper, S. Herden, D. Bortis, and J. Kolar, "Impact of PV string shading conditions on panel voltage equalizing converters and optimization of a single converter system with overcurrent protection," in *2014 16th European Conference on Power Electronics and Applications (EPE'14-ECCE Europe)*, Aug. 2014, pp. 1–10.

[89] I. Novak, K. Williams, J. Miller, G. Blando, and N. Shannon, "Dc and ac bias dependence of capacitors," in *DesignCon 2011*, Jan. 2011.

[90] *The Effect of Temperature and Voltage Changes on High Voltage Ceramic Capacitors*, CalRamic Technologies LLC, 2023, Application Note - AN110. [Online]. Available: https://www.calramic.com/Design/Assets/PDF_files/AN110-Voltage-Temperature-Coefficient.pdf

[91] P. S. Bullen, *Handbook of Means and Their Inequalities*. Dordrecht: Springer Netherlands, 2003, ch. 3, pp. 175–178. [Online]. Available: https://doi.org/10.1007/978-94-017-0399-4_3

[92] S. Sykora, "Means and averages - basic properties," Jul. 2009. [Online]. Available: http://www.ebyte.it/library/docs/math09/Means.html

[93] G. Strang, *Linear Algebra and Its Applications*, 4th ed. Thomson, Brooks/Cole, 2006.

[94] N. Madavan, "A NASA perspective on electric propulsion technologies for commercial aviation," in *2016 International Conference on Electrical Systems for Aircraft, Railway, Ship Propulsion and Road Vehicles & International Transportation Electrification Conference*, Nov. 2016. [Online]. Available: https://ntrs.nasa.gov/api/citations/20180008723/downloads/20180008723.pdf

[95] P. Wheeler, T. S. Sirimanna, S. Bozhko, and K. S. Haran, "Electric/hybrid-electric aircraft propulsion systems," *Proc. IEEE*, vol. 109, pp. 1115–1127, Jun. 2021.

[96] N. Pallo, T. Foulkes, T. Modeer, S. Coday, and R. Pilawa-Podgurski, "Power-dense multilevel inverter module using interleaved GaN-based phases for electric aircraft propulsion," *2018 IEEE Applied Power Electronics Conference and Exposition (APEC)*, Mar. 2018.

[97] T. Modeer, N. Pallo, T. Foulkes, C. B. Barth, and R. C. N. Pilawa-Podgurski, "Design of a GaN-based interleaved nine-level flying capacitor multilevel inverter for electric aircraft applications," *IEEE Trans. Power Electron.*, vol. 35, pp. 12 153–12 165, Nov. 2020.

[98] S. Coday, N. Ellis, N. Stokowski, and R. C. Pilawa-Podgurski, "Design and implementation of a (flying) flying capacitor multilevel converter," in *2022 IEEE Applied Power Electronics Conference and Exposition (APEC)*, Mar. 2022, pp. 542–547.

[99] S. Coday, E. Krause, M. E. Blackwell, N. M. Ellis, A. Barchowsky, and R. C. Pilawa-Podgurski, "Design and implementation of a GaN-based capacitively-isolated hybrid dickson switched-capacitor dc-dc converter for space applications," in *2023 IEEE Applied Power Electronics Conference and Exposition (APEC)*, Mar. 2023, pp. 3154–3159.

[100] C. Chatfield, "Model uncertainty, data mining and statistical inference," *Journal of the Royal Statistical Society: Series A (Statistics in Society)*, vol. 158, pp. 419–444, 1995. [Online]. Available: https://rss.onlinelibrary.wiley.com/doi/abs/10.2307/2983440

[101] A. C. Aitken, "IV. on least squares and linear combination of observations," *Proceedings of the Royal Society of Edinburgh*, vol. 55, pp. 42–48, Sep. 1936.

[102] S. Greenland *et al.*, "Statistical tests, P values, confidence intervals, and power: a guide to misinterpretations," *European Journal of Epidemiology*, vol. 31, pp. 337–350, May 2016.

[103] *Aluminum Electrolytic Capacitor Application Guide*, Cornell Dubilier Electronics, 2023, [Online] Available at www.cde.com.

[104] J. Azurza Anderson, G. Zulauf, P. Papamanolis, S. Hobi, S. Mirić, and J. W. Kolar, "Three levels are not enough: Scaling laws for multilevel converters in ac/dc applications," *IEEE Trans. Power Electron.*, vol. 36, pp. 3967–3986, Apr. 2021.

[105] P. Wang, D. Giuliano, S. Allen, and M. Chen, "MSC-PoL: An ultra-thin 220-A/48-to-1-V hybrid GaN-Si CPU VRM with multistack switched capacitor architecture and coupled magnetics," in *2023 IEEE Applied Power Electronics Conference and Exposition (APEC)*, May 2023, pp. 1967–1974.

[106] Y. Zhu, T. Ge, N. M. Ellis, L. Horowitz, and R. C. N. Pilawa-Podgurski, "A 500-A/48-to-1-V switching bus converter: A hybrid switched-capacitor voltage regulator with 94.7% peak efficiency and 464-W/in3 power density," in *2023 IEEE Applied Power Electronics Conference and Exposition (APEC)*, May 2023, pp. 1989–1996.

[107] Z. Ye, S. R. Sanders, and R. C. N. Pilawa-Podgurski, "Modeling and comparison of passive component volume of hybrid resonant switched-capacitor converters," *IEEE Trans. Power Electron.*, vol. 37, pp. 10 903–10 919, Sep. 2022.

[108] N. M. Ellis, N. C. Brooks, M. E. Blackwell, R. A. Abramson, S. Coday, and R. C. N. Pilawa-Podgurski, "A general analysis of resonant switched capacitor converters using peak energy storage and switch stress including ripple," *IEEE Trans. Power Electron.*, pp. 1–21, 2023.

[109] C. R. Sullivan and S. R. Sanders, "Design of microfabricated transformers and inductors for high-frequency power conversion," *IEEE Trans. Power Electron.*, vol. 11, pp. 228–238, Mar. 1996.

[110] S. R. Pasternak, M. H. Kiani, J. S. Rentmeister, and J. T. Stauth, "Modeling and performance limits of switched-capacitor dc–dc converters capable of resonant operation with a single inductor," *IEEE Trans. Emerg. Sel. Topics Power Electron.*, vol. 5, pp. 1746–1760, Dec. 2017.

Nathan Charles Brooks (Member, IEEE) is currently an Assistant Professor in the Electrical and Computer Engineering Department at the Rose-Hulman Institute of Technology in Terre Haute, IN, USA. He received the B.S. degree in electrical engineering from the Rose-Hulman Institute of Technology in 2016, the M.S. degree in electrical engineering from the University of Illinois at Urbana-Champaign, IL, USA, in 2018, and the Ph.D. degree in electrical engineering and computer sciences at the University of California at Berkeley, CA, USA, in 2023. His research interests include dynamic modeling of switched circuits, high-performance circuit layout, passive component characterization, and high-density design of single-phase and multilevel power converters. His teaching interests include introductory circuit analysis, introductory control systems, signal processing, and power electronics.

Jiarui Zou (Student Member, IEEE) earned his B.S. degree in Electrical Engineering from the University of Illinois Urbana-Champaign, IL, USA in 2021. He is currently pursuing his Ph.D. in Electrical Engineering at the University of California, Berkeley, CA. His research interests include high-performance hybrid switched-capacitor converters, custom magnetics design automation, high-performance circuit layout, and assembly techniques, as well as circuit component performance analysis. He received the IEEE COMPEL Best Paper Award in 2023.

Samantha Coday (Member, IEEE) received the B.S. degree in electrical engineering and mathematics from Southern Methodist University, TX, USA, in 2017. She completed the M.S. degree and Ph.D. degree in electrical engineering and computer sciences in 2019 and 2023, respectively, from the University of California, Berkeley, CA, USA. Dr. Coday joined Massachusetts Institute of Technology in 2023 as an Assistant Professor of Electrical Engineering and a Principal Investigator in the Research Laboratory of Electronics. Her research interests include hybrid switched-capacitor circuits focusing on the design and implementation of converters in harsh aerospace environments. Dr. Coday has received the Outstanding Graduate Student Instructor Award at University of California, Berkeley, the Cadence Women in Technology Scholarship and the ThinkSwiss Research Scholarship.

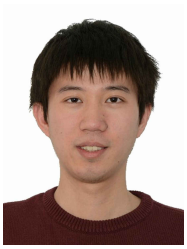

Ting Ge (Member, IEEE) (S'13-M'19) received the B.S. degree in Electrical Engineering from Huazhong University of Science and Technology, Wuhan, China in 2012, and the M.S. and Ph.D. degrees in Electrical Engineering from Virginia Tech, Blacksburg, VA, USA, in 2017 and 2018, respectively. He was a Post-doctoral researcher in the University of California, Berkeley, from 2020 to 2022, with a focus on hybrid switched-capacitor converters and magnetic design. He is currently, since 2022, an R&D manager at Monolithic Power Systems, San Jose, CA, with a focus on voltage regulator power module development for high-performance computing and AI applications.

Nathan Miles Ellis (Member, IEEE) was born in Cork, Ireland. He received the B.S. degree in Electrical and Electronic Engineering from the University College Cork, Ireland, in 2013, and the M.S. and Ph.D degrees in Electrical and Computer Engineering from the University of California, Davis in 2017 and 2020 respectively. During this time, he was funded in part by both Texas Instruments and the U.S. Dept. of Education in recognition of research excellence in areas of national need.

Dr. Ellis is currently with the University of California, Berkeley within the Department of Electrical Engineering and Computer Sciences. His primary area of research is power electronics where he is an author on over 30 journal and conference publications. His interests include vehicle electrification, renewable energy integration, datacenter power delivery, biomedical devices, aerospace, and mixed signal integrated circuit design. He is an author on two IEEE prize papers.

Robert C. N. Pilawa-Podgurski (Fellow, IEEE) (S'06–M'11–SM'19-F'24) was born in Hedemora, Sweden. He is currently a Professor in the Electrical Engineering and Computer Sciences Department at the University of California, Berkeley. Previously, he was an Associate Professor in Electrical and Computer Engineering at the University of Illinois Urbana-Champaign. He received dual B.S. degrees in physics and electrical engineering and computer science in 2005, the M.Eng. degree in electrical engineering and computer science in 2007, and the Ph.D. degree in electrical engineering in 2012, all from the Massachusetts Institute of Technology. He performs research in the area of power electronics, and enjoys swimming. His research interests include renewable energy applications, electric vehicles, CMOS power management, high density and high efficiency power converters, datacenter power delivery, and advanced control of power converters.

Dr. Pilawa-Podgurski served as the Student Activities Chair for IEEE Energy Conversion Congress and Exposition 2016 & 2017, and as the Technical Co-Chair for the 4th IEEE Workshop on Wide Bandgap Power Devices and Applications, 2016. From 2014 to 2022, he served the PELS Technical Committee 6 – Emerging Power Electronics Technologies as Awards Chair, Secretary, Vice Chair, and Chair. From 2016-2019 he served as Chair of PELS Technical Committee 2—Power Conversion Systems and Components. From 2014-2019, he served as Associate Editor for IEEE Transactions on Power Electronics, and for IEEE Journal of Emerging and Selected Topics in Power Electronics. From 2018-2023, he was a member of the IEEE ISSCC Power Management Committee.

Dr. Pilawa-Podgurski received the Chorafas Award for outstanding MIT EECS Master's thesis, the Google Faculty Research Award in 2013, and the 2014 Richard M. Bass Outstanding Young Power Electronics Engineer Award of the IEEE Power Electronics Society, given annually to one individual for outstanding contributions to the field of power electronics before the age of 35. In 2015, he received the Air Force Office of Scientific Research Young Investigator Award, the UIUC Dean's Award for Excellence in Research in 2016, the UIUC Campus Distinguished Promotion Award in 2017, and the UIUC ECE Ronald W. Pratt Faculty Outstanding Teaching Award in 2017. He was the 2018 recipient of the IEEE Education Society Mac E. Van Valkenburg Award given for outstanding contributions to teaching unusually early in his career. In 2023, he received the UC Berkeley EECS department Electrical Engineering Outstanding Teaching Award. He is co-author of fifteen IEEE prize papers.